Front. Earth Sci. 2021, 15(2): 310–331
https://doi.org/10.1007/s11707-021-0892-y

RESEARCH ARTICLE

Geological controls of shale gas accumulation and enrichment mechanism in Lower Cambrian Niutitang Formation of western Hubei, Middle Yangtze, China

Lulu XU[1], Saipeng HUANG (✉)[2,3], Zaoxue LIU[1], Yaru WEN[1], Xianghui ZHOU[1], Yanlin ZHANG[1], Xiongwei LI[1], Deng WANG[1], Fan LUO[1], Cheng CHEN[4]

1 Hubei Geological Survey, Wuhan, Hubei 430034, China
2 Key Laboratory of Continental shale Accumulation and Development of Ministry of Education, Northeast Petroleum University, Daqing 163318, China
3 Coal Reservoir Laboratory of National Engineering Research Center of CBM Development & Utilization, School of Energy Resources, China University of Geosciences, Beijing 100083, China
4 The Seventh Geological Brigade of Hubei Geological Bureau, Yichang 443000, China

Abstract The lower Cambrian Niutitang Formation is of crucial importance for shale gas target reservoirs in western Hubei, China; however, little work has been done in this field, and its shale gas accumulation and enrichment mechanism are still unclear. Based on survey wells, outcrop data, and large numbers of tests, the geological conditions of shale gas accumulation were studied; moreover, the factors that influence the gas content were thoroughly discussed. The results show that the Niutitang Formation (ϵ_1n) can be divided into three sections: the first section (ϵ_1n^1), the second section (ϵ_1n^2), and the third section (ϵ_1n^3). The ϵ_1n^2 is the main shale gas reservoir. The deep shelf facies is the main sedimentary facies and can be divided into three main lithofacies: argillaceous siltstone, carbonaceous shale and carbonaceous siliceous rock. The total organic carbon (TOC) content shows gentle growth trends until bottom of the ϵ_1n^2 and then decreases rapidly within the ϵ_1n^1, and the TOC content mainly ranges from 2% to 4% horizontally. The calcite and dolomite dissolution pores, clay intergranular pores and organic pores are the main pore types and the micropore types are clearly related to the mineral compositions and the TOC content. Vertically, the gas content is mainly affected by the TOC content. Horizontally, wells with high gas contents are distributed only southeast of the Huangling anticline, and the combination of structural styles, fault and fracture development, and the distribution of the regional unconformity boundary between the upper Sinian Dengying Formation (Z_2d) and the ϵ_1n^2 are the three most important factors affecting the gas content. The favorable areas must meet the following conditions: a deep shelf environment, the presence of the ϵ_1n^1, wide and gentle folds, far from large normal faults that are more than 5 km, moderate thermal evolution, and greater than 500 m burial depth; this includes the block with the YD2–ZD2 wells, and the block with the Y1 and YD4 wells, which are distributed in the southern portion of the Huangling anticline and northern portion of the Xiannvshan fault.

Keywords shale gas, Niutitang Formation, accumulation conditions, factors influencing the gas content, sedimentary facies

1 Introduction

Shale gas is an important unconventional oil and gas resource in the world (Curtis, 2002; Bowker, 2007; Hughes, 2013; Li et al., 2019a; Li et al., 2020; Zheng et al., 2020). China is one of the countries with the largest shale gas reserves in the world, and the Sichuan Basin is currently the most important area for the commercial development of shale gas (Hao et al., 2013; Guo and Zhang, 2014; Tang et al., 2019; Nie et al., 2020). The Niutitang Formation (ϵ_1n) and lower Silurian Longmaxi marine shales are two main shale gas target layers (EIA, 2011; Zou et al., 2014). They are generally characterized by a wide distribution, large thickness, and high content of the total organic carbon (TOC) (Zhang et al., 2008; Jin et al., 2018; Yi et al., 2019). However, little research work

Received November 11, 2020; accepted March 24, 2021

E-mail: huangspcugb@hotmail.com

has been carried out on shale gas accumulation and the factors influencing the gas content in the $\epsilon_1 n$ in western Hubei compared with the Longmaxi Formation. Limited studies have shown that a shallow carbonate ramp, and shallow and deep shelves constitute the sedimentary environment of the $\epsilon_1 n$, and a deep shelf environment is the basic condition for shale gas accumulation (Wang et al., 2013). Carbonaceous shale is the main lithology of the $\epsilon_1 n$ with minor amounts of siltstone and limestone (Huang et al., 2012); The TOC and vitrinite reflectance (R_o) values are generally greater than 2.0% and 3.0%, respectively (Zhao et al., 2016). The $\epsilon_1 n$ is characterized by a high amount of brittle minerals, and low porosity and permeability (Huang et al., 2018). The shale reservoir is dominated by nanometre pores and inter-granular pores, organic as well as some dissolution pores are the main micropore types that provide the reservoir space for shale gas (Nie et al., 2014). Studies have showed that the gas content of the lower part is higher than that of the upper part of the $\epsilon_1 n$ due to the high TOC value and large amount of brittle mineral (Tan et al., 2014). Although the accumulation of shale gas is influenced by many factors, preservation condition are the most important factors for shale gas enrichment (Ambrose et al., 2010; Roger and Neal, 2011; Loucks et al., 2012; Zeng et al., 2016). A good sealing capacity of roofs and floors, moderate burial depth and low development of normal faults are beneficial for the shale gas accumulation (Nie et al., 2012).

Although the mechanism of shale gas accumulation in the $\epsilon_1 n^2$ of western Hubei has received limited study, there are still three questions that remain. First, there are few studies on the lithofacies division of the deep shelf strata considering its wide distribution. Second, the vertical heterogeneity of shale reservoirs needs to be further studied. Third, the main vertical and horizontal controlling factors of shale gas content vertically and horizontally need to be clarified. Therefore, the black shale in the $\epsilon_1 n$ of western Hubei is chosen for this paper, and several methods are conducted. The rock lithology and sedimentary facies are researched, and shale gas accumulation conditions, such as shale thickness, burial depth, geochemistry and reservoir physical properties are discussed. Moreover, the gas content and its factors that influence it are analyzed. Finally, the favorable area is determined according to the characteristic analysis of sedimentation, burial depth, shale thickness, TOC, R_o, and gas content and its impact factors.

2 Geological setting

The study area is located in the north-central Yangtze Region, adjacent to the Sichuan Basin and Hunan Province, it is bounded by the northern Xiangguang fault (F6) and eastern Tongchenghe fault (F12) with exposed strata from the Proterozoic Nanhua to the Cenozoic Neogene system; it is a marine and continental superimposed plate. The folds are mainly NE-SW-oriented (B1–B6, B8), and a few are nearly E-W-oriented (B7, B9–B11). The faults are mainly NE-SW-oriented (F1–F5, F8). However, there are also a few NW-SE-oriented (F9–F12) and E-W-oriented (F6 and F7) faults (Fig. 1). There are four sets of marine hydrocarbon source rocks in the Middle Yangtze Region: lower Sinian, lower Cambrian, upper Ordovician–lower Silurian and upper Permian source rocks. Currently, the large-scale lower Cambrian $\epsilon_1 n^2$ shale is one of the most important shale gas reservoirs, with a 0–300 m interval of black shale and a high content of TOC due to favorable sedimentary facies.

3 Data and methodology

A total of 29 shale gas wells and 18 outcrop sections were chosen in the study area. Nearly 400 samples obtained from 16 wells were tested for TOC, R_o, mineral composition, porosity, permeability, micropore structure, field canister desorption gas content (V_D), residual gas content (V_R) and Langmuir volume (V_L). Specifically, due to the high gas content of the drilling core, the 23 samples from the ZD2 well were used to study the variations in the lithology, geochemistry, reservoir physical properies and gas-bearing properties in the longitudinal direction. The TOC content was tested by a Leco CS-230 carbon-sulfur tester. The mineral composition was tested by an X'Pert PRO DY2198 X-ray diffractometer. Porosity and permeability were tested by an AP-608 overpressure porosity permeability tester. Microscopic pores were observed by a JSM-35CF scanning electron microscope. Moreover, V_L was tested by a GAI-100 high-pressure isothermal adsorption apparatus. V_D was tested by a YSQ-IV Rock desorption apparatus. V_R was tested by an FCG009 shale gas field testing apparatus. All the samples were tested in the State Key Laboratory of Geological Processes and Mineral Resources. Based on the test data and core observation, the geological conditions for shale gas accumulation and the enrichment mechanism of the $\epsilon_1 n$ in western Hubei were studied.

4 Results

4.1 Strata and sedimentary facies

The ZD2 well located in the southeastern Huangling anticline (B8) was chosen to study the characteristic of strata and sedimentary facies of the $\epsilon_1 n$ (Fig. 2). According to the lithological characteristics of the ZD2 well, the $\epsilon_1 n$ can be vertically divided into 3 sections: the first section ($\epsilon_1 n^1$), the second section ($\epsilon_1 n^2$), and the third section ($\epsilon_1 n^3$). The lower part of $\epsilon_1 n^1$ is argillaceous siltstone, and the upper part is mainly carbonaceous limestone mixed

with a minor amount of carbonaceous shale; thus, the sedimentary environment was a shallow shelf. The lithology of the $\epsilon_1 n^2$ is mainly carbonaceous shale with a minor amount of silty mudstone; thus, the sedimentary environment was a deep shelf. The lithology of the $\epsilon_1 n^3$ is mainly limestone mixed with carbonaceous shale and argillaceous siltstone, and thus the sedimentary environment was a shallow shelf.

The lithofacies paleo-geographic map of the $\epsilon_1 n^2$ in the study area is derived from the lithology and thickness of 29 shale gas wells and 18 outcrop sections. The lithofacies paleo-geographic map shows that there is a paleo-continent in the northeast and that the $\epsilon_1 n$ is absent in this area. From east to west, the sedimentary facies of the $\epsilon_1 n^2$ are carbonate slope, shallow shelves with lithologies of limestone, dolomite and carbonaceous shale, deep shelves with carbonaceous shale, shallow shelves with the lithologies of limestone and silty mudstone. Three submarine uplifts are located north of Yichang city on the shallow shelf. Morphologically, the deep shelf is horn-shaped, wide at both ends and narrow in the middle. The deep shelf has a wide distribution, from western Lichuan city to eastern Yichang city and from northern Shengnongjia to southern Hefeng counties. The deep shelf can be divided into three parts according to lithological characteristics: the northern part is mainly

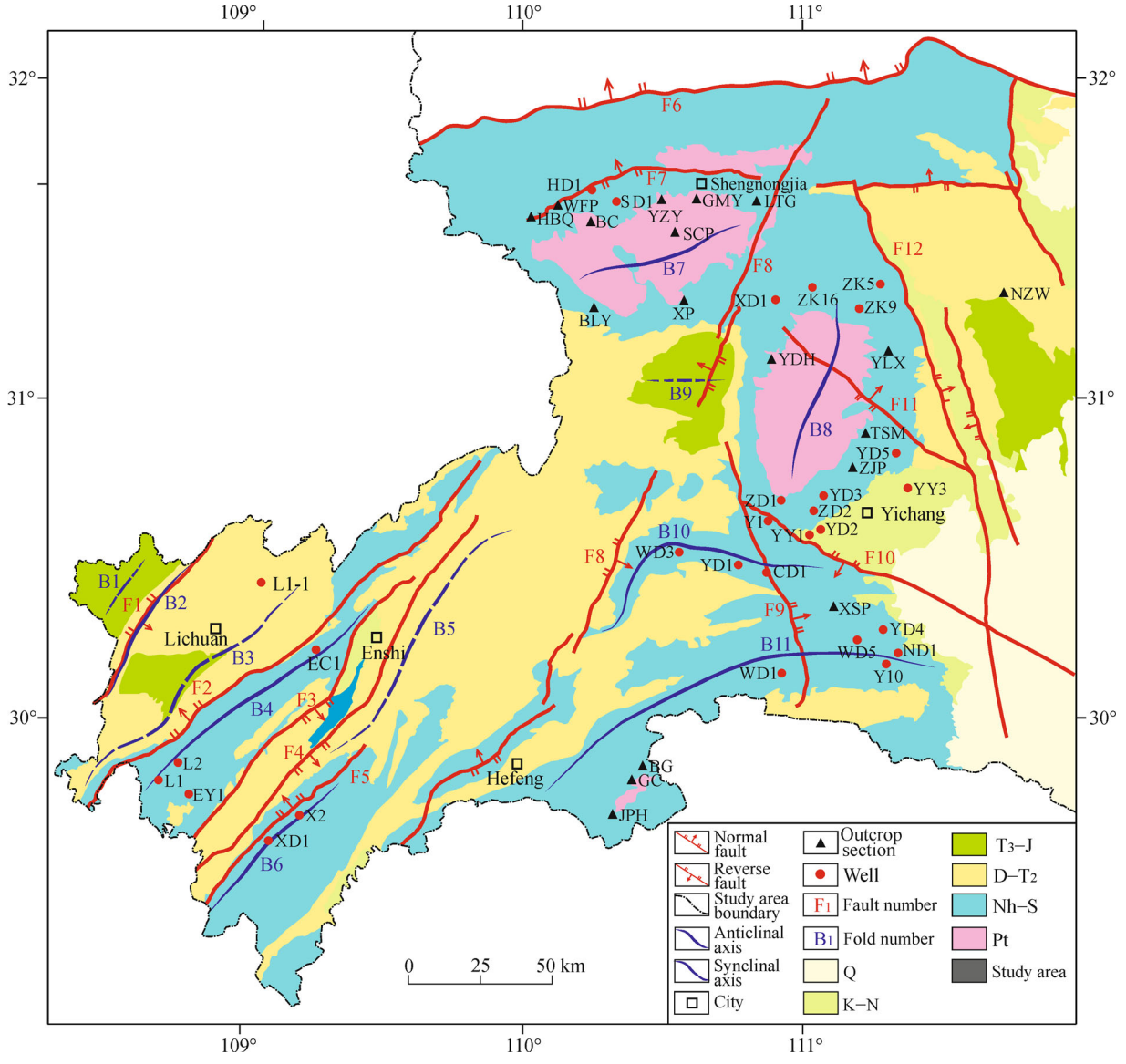

Fig. 1 Location, tectonic setting of lower Cambrian Niutitang shale in western Hubei, Middle Yangtze Region. Notation: F1-Qiyueshan Fault; F2-Jianshi Fault; F3-Enshi Fault; F4-Daqingshan Fault; F5-Xianfeng Fault; F6-Xiangguang Fault; F7-Yangri Fault; F8-Xinhua Fault; F9-Xiannvshan Fault; F10-Tianyangping Fault; F11-Wuduhe Fault; F12-Tongchenghe Fault; B1-Shizhu syncline; B2-Qiyueshan anticline; B3-Lichuan syncline; B4-Zhongyang anticline; B5-Huaguoping syncline; B6-Xianfeng anticline; B7-Shengnongjia anticline; B8-Huangling anticline; B9-Zhigui syncline; B10-Changyang anticline; B11-Yidu-Hefeng anticline.

carbonaceous shale mixed with argillaceous siltstone, the middle part is mainly carbonaceous shale and the south part is carbona-ceous shale mixed with silicious rock. In general, siltstone gradually decreases as silicious rock increases from north to south (Fig.3).

4.2 Thickness and burial depth of organic-rich shale

There are two main deposits centers with large thicknesses. The first deposit is distributed in southern Enshi city with a thickness of greater than 200 m, and the thickness gradually increases to the south. The other area is in north-western Shengnongjia with a thickness of greater than 250 m, and the thickness gradually increases to the north. The thickness of the shale is relatively thin to the east of Yichang and west of Lichuan, with a thickness of mainly 10–50 m, and in some areas, the thickness of the shale is less than 10 m, such as in wells XD1, YD3, YD5 and ZK9. The burial depths of the Lichuan and Huaguoping synclines (B3 and B5) mainly range from 2000 to 4000 m, and other areas, such as the Shengnongjia, Huangling, and Hefeng anticlines (B7, B8, and B11) have burial depths of mainly less than 2000 m (Fig. 4).

4.3 Shale reservoir characteristics

According to the classification criteria of shale gas

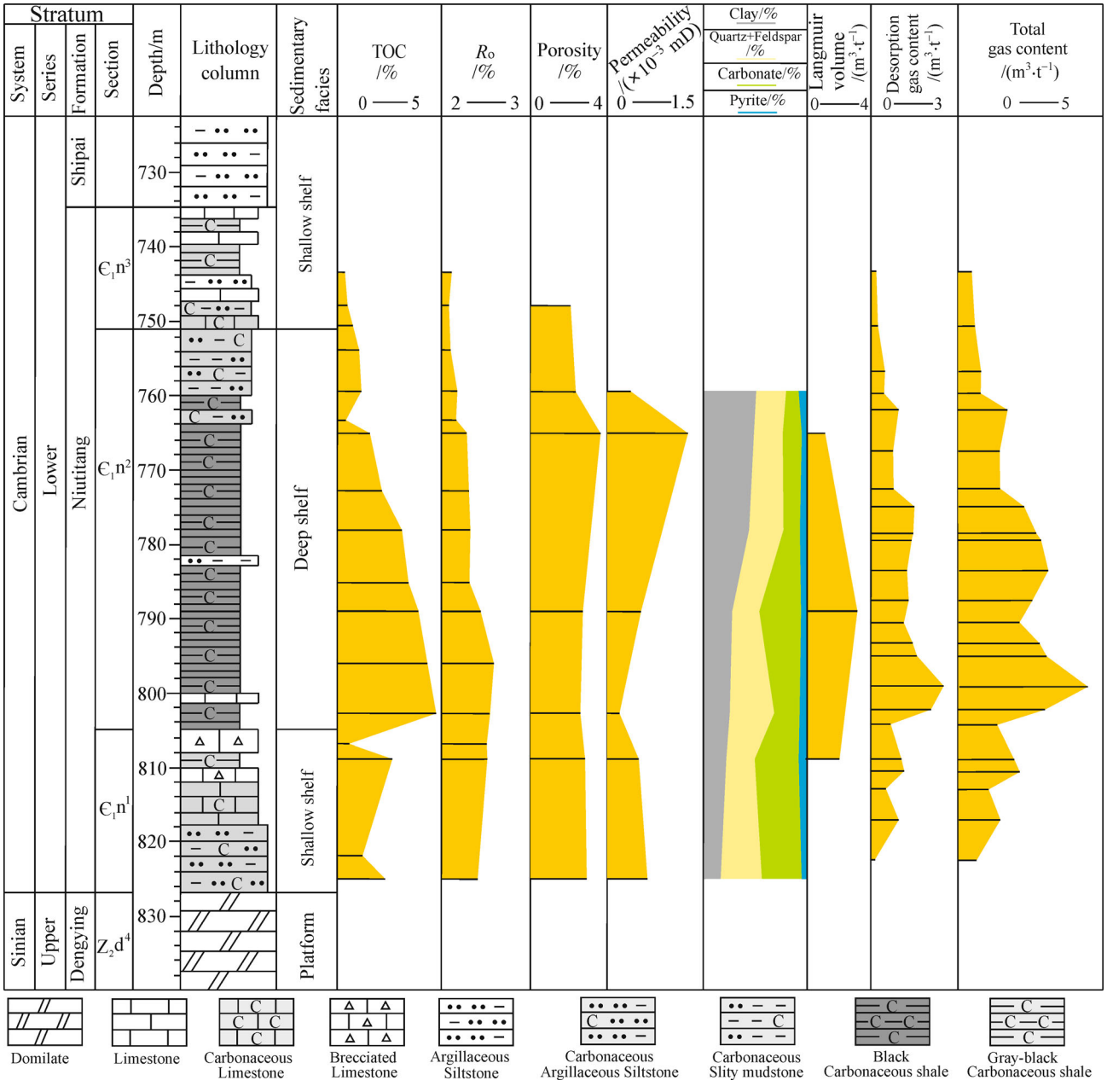

Fig. 2 Composite stratigraphic column compiled from representative well ZD2 for the lower Cambrian ϵ_1n in western Hubei.

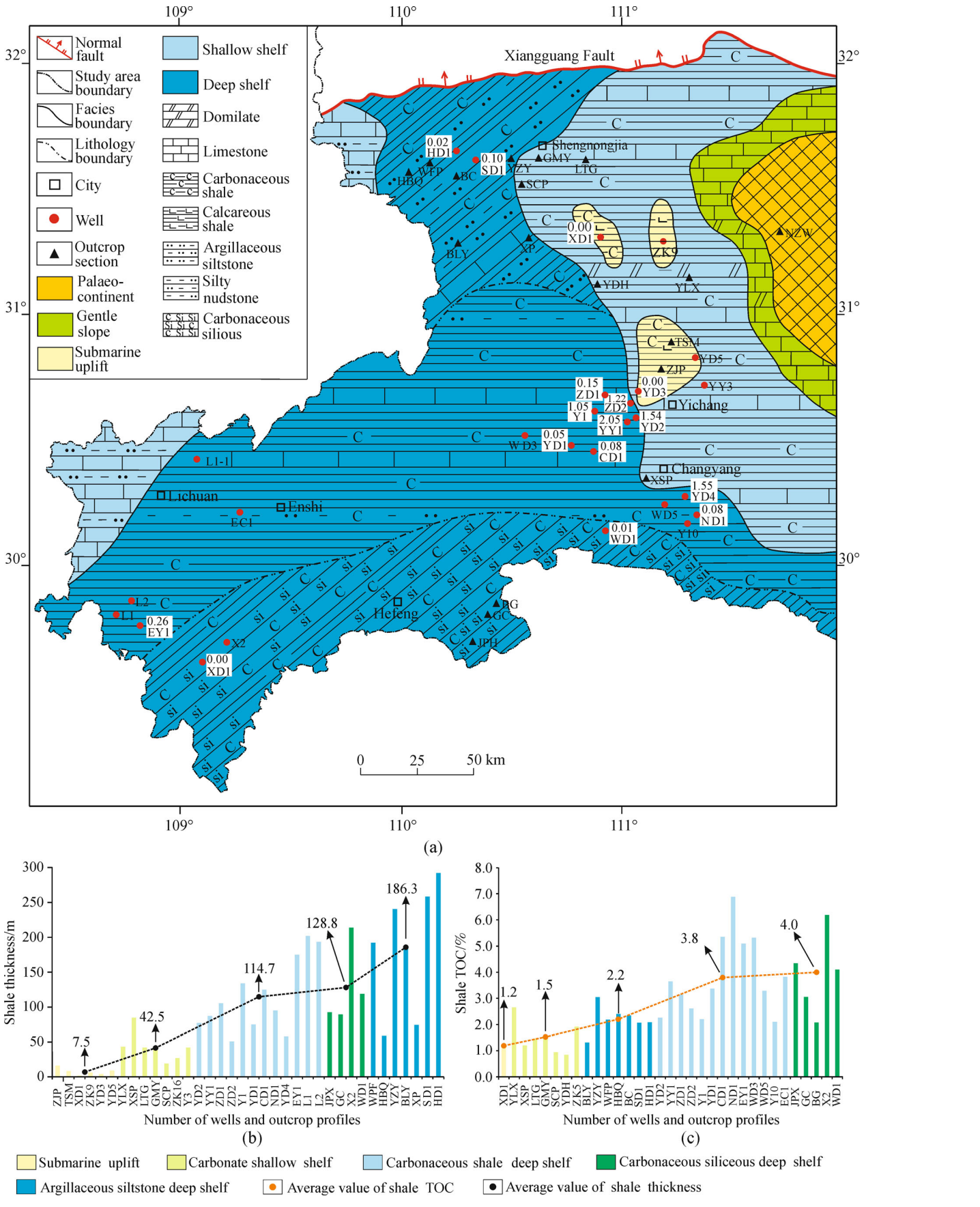

Fig. 3 Lithofacies paleo-geographic of the $\epsilon_1 n^2$ and its influence on the thicknesses, TOC, and gas content of organic-rich shale in western Hubei. (a) Lithofacies paleo-geographic of the $\epsilon_1 n^2$ and its influence on gas content; (b) the influence of sedimentary facies on the thicknesses of organic-rich shale; (c) the influence of sedimentary facies on TOC of organic-rich shale.

evaluation parameters in the Technical Specification for the Calculation and Evaluation of Shale Gas Reserves (DZ/T0254-2014) which was issued by the National Ministry of Natural Resources (Table 1), the shale reservoir characteristics of the $\in_1 n^2$ were analyzed by TOC, R_o, mineral composition, porosity, permeability and microscopic pores and fractures.

4.3.1 Organic geochemical characteristics

The vertical variations in TOC and R_o for the ZD2 well were studied. The results showed that the TOC ranges from 0.4%–5.0%, and the average TOC values of the $\in_1 n^1$, $\in_1 n^2$, and $\in_1 n^3$ are 1.67%, 2.61%, and 0.45%, respectively. The TOC shows a gentle growth trend until the bottom of the $\in$

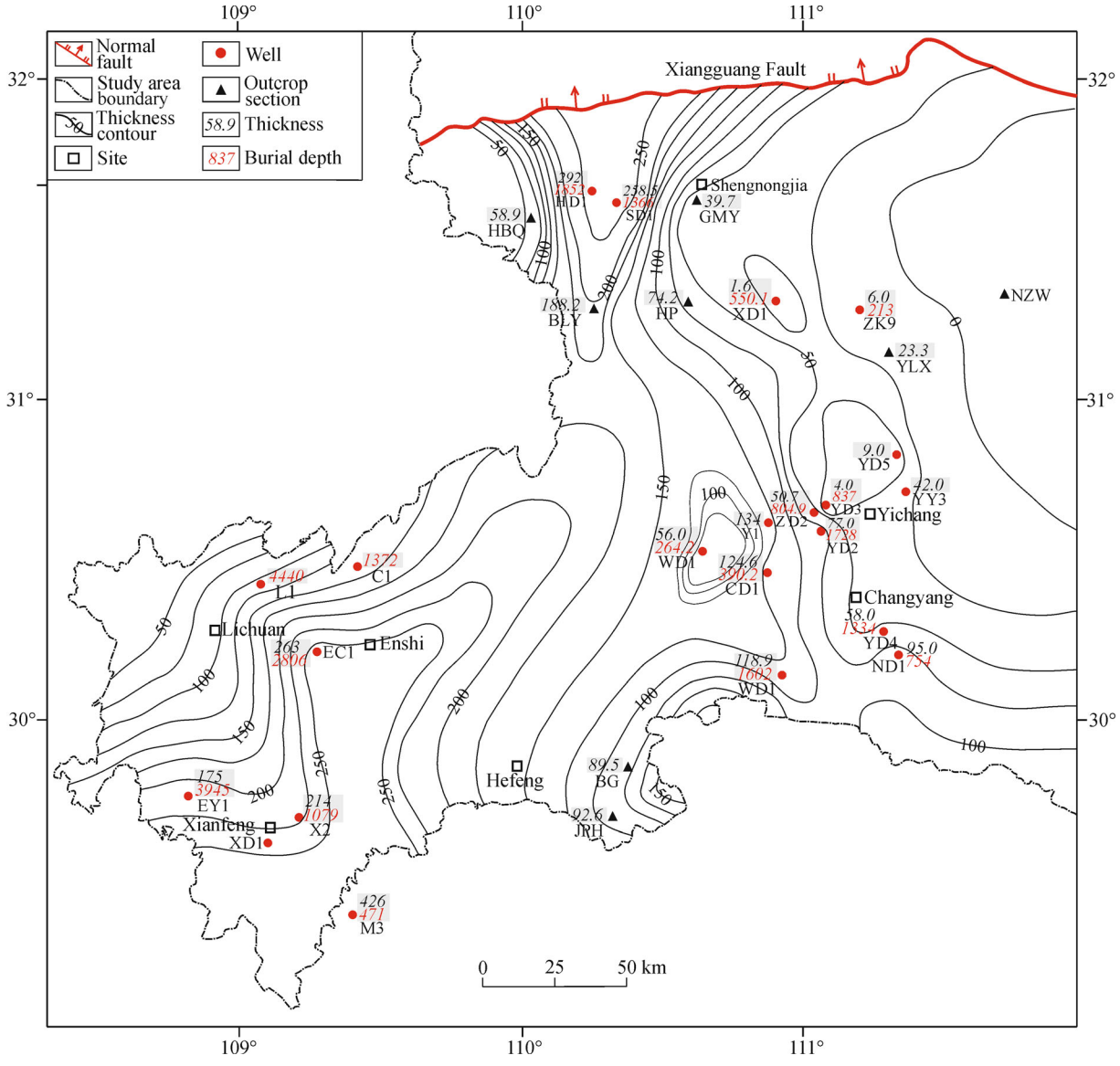

Fig. 4 Organic-rich shale thickness contour map of the $\in_1 n^2$ in western Hubei.

Table 1 Classification criteria of shale gas evaluation parameters (DZ/T0254-2014)

Parameters	Extra-high	High	Medium	Low	Ultra-low
TOC (%)	≥4.0	2.0–4.0	1.0–2.0	⩽1.0	/
R_o (%)	/	≥2.0	1.3–2.0	< 1.3	/
Brittle mineral (%)	/	≥40	30–40	< 30	/
Porosity (%)	/	≥10	5–10	2–5	< 2
Permeability (mD)	/	≥100	10–100	1–10	< 1

Note: "/" indicates that there are no classification criteria.

$_1n^2$ and then decreases rapidly within the ϵ_1n^1. The ϵ_1n^2 with an average TOC value of 2.61% is the main hydrocarbon source rock of the ϵ_1n and is the most important target layer in this study. The R_o value ranges from 2.05%–2.59% and generally increases along with burial depth (Fig. 2).

Date from the 368 TOC and 89 R_o samples showed that the samples with high TOC values of 2.0%–4.0% accounted for the largest proportion, followed by the samples with very high TOC values that are higher than 4.0% and medium TOC values of 1.0%–2.0% (Fig. 5(a)). The high maturity samples with R_o between 2.0%–3.5% accounted for the larger proportion (Fig. 5(b)). According to the TOC contour map, the high TOC values are mainly distributed in 3 areas, including Enshi city to Hefeng county, Shengnongjia and Changyang county with TOC values mainly ranging from 3%–5%. In general, TOC values are higher in the middle of the study area and decrease significantly to the west of Lichuan city and to the east of Yichang city. The distribution of R_o is similar to that of TOC, with the highest value more than 4% in Hefeng county (Fig. 5(c)).

4.3.2 Mineral composition and content

Previous studies indicate that clay mineral content affects the specific surface area and adsorption capacity of shales (Aringhieri, 2004; Cheng and Huang, 2004; Chalmers and Bustin, 2008). In addition, shale rich in brittle minerals more easily forms hydraulic fractures (Bowker, 2003;

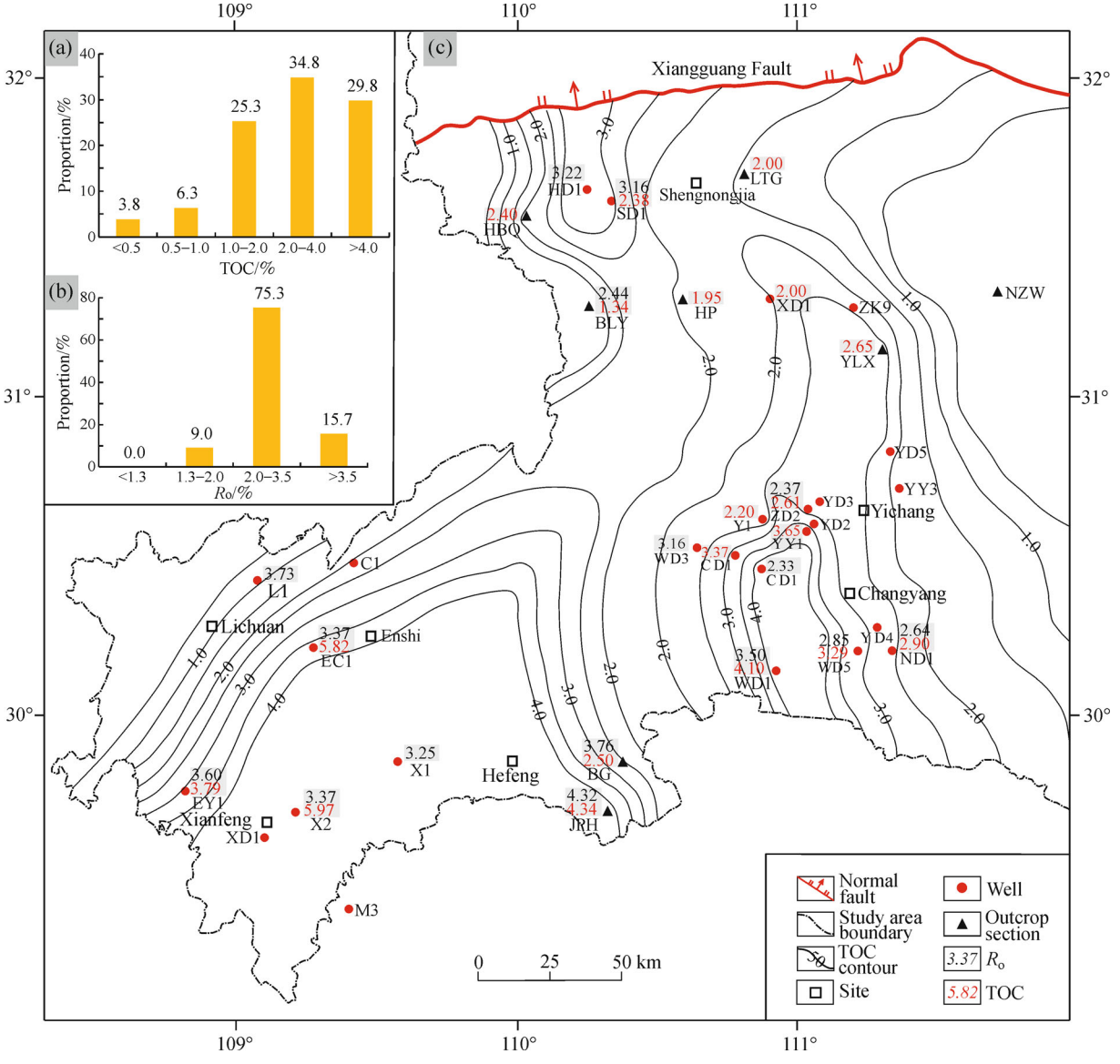

Fig. 5 TOC and R_o distribution characteristics of organic-rich shale of the ϵ_1n^2 in study area. (a) The proportion of different TOC intervals; (b) The proportion of different R_o value intervals; (c) TOC contour map of organic-rich shale of the ϵ_1n^2.

Jarvie et al., 2007). Therefore, the analysis of shale mineral composition is of great significance to the exploration and development of shale gas. According to the mineral composition, the shale lithofacies classification scheme can be divided into siliceous shale, calcareous shale, clay shale and mixed shale and then subdivided into 31 subclasses (Wang et al., 2018). The results show that siliceous shale (S) is the main lithofacies in most samples, followed by mixed shale (M), calcareous shale (C) and clay shale (CM) which rarely occur in the samples (Fig. 6(a)). Additionally, the average brittle mineral content is 52.5%, which is based on 89 samples that belong to the high level according to the classification criteria in Table 1. Clay content decreases and quartz content slightly increases with burial depth (Figs. 6(b), 6(c), and 6(d)). Moreover, the mineral composition has different characteristics in different areas. The SD1 well in the northern part of the study area contains the least clay minerals (Fig. 6(b)), the ZD2 well in the middle part of the study area contains relatively more carbonate and pyrite minerals (Fig. 6(c)), and the GC outcrop section in the south contains relatively more quartz and nearly no carbonate minerals (Fig. 6(d)).

4.3.3 Porosity and permeability

As fine-grained sedimentary rocks, shale reservoirs generally have low porosity and permeability (Best and Katsube, 1995; Clarkson et al., 2013; Chalmers and Bustin, 2015; Liu and Ostadhassan, 2019). Taking well ZD2 as an example, the changes in the porosity and permeability of the $\epsilon_1 n^2$ in the vertical direction are analyzed. The results show that the porosity values range from 1.95% to 3.72% with little vertical change; the permeability values range from 0.00017 to 0.00186 md with great vertical change (Fig. 2). According to the classification criteria, the porosity for most samples with low level values is distributed in the 2%–5% interval, followed by the samples with ultra-low level values of less than 2% (Fig. 6(e)). The permeabilities of all samples are less than 1 mD, which indicates an ultra-low level (Fig. 6(f)).

4.3.4 Microscopic pore structure

The pore structure of shale is an important factor affecting the gas storage capacity of shale reservoirs and the commercial exploitation of shale gas (Ross and Bustin, 2009; Curtis et al., 2012a; Chalmers et al., 2012; Clarkson et al., 2013; Li et al., 2016; Tang et al., 2016; Li et al., 2019b). The micropore types, structures and sizes of the rock can be precisely evaluated by argon ionizer polishing and scanning electron microscopy (SEM) (Curtis et al., 2012b; Zhao et al., 2014; Li et al., 2018). Two samples in the upper and middle parts of the $\epsilon_1 n^2$ were observed by SEM. Sample A in the upper part of the $\epsilon_1 n^2$ with a TOC value of 1.02% and a brittle mineral content of 48% contains calcite dissolution pores, clay intergranular pores and a few organic pores. The calcite dissolution pores are mainly elliptical with apertures of 0.2–1 μm and some pores are long strips (Fig. 7(A1)). The pyrite intergranular pores (Fig. 7(A2)) and the quartz inter-crystal pores are poorly developed (Fig. 7(A3)). The clay intergranular pores are mainly elliptical with apertures of 0.5–2.0 μm (Fig. 7(A4)). The organic matter pores are relatively less developed with irregular and elliptical shapes, and the pore sizes range from 30–100 nm (Figs. 7(A5) and 7(A6)). Sample B in the middle of the $\epsilon_1 n^2$ with a TOC value of 3.16% and a brittle mineral content of 56% contains calcite and dolomite dissolution pores, clay intergranular pores, pyrite intergranular pores and organic pores. The calcite dissolution pores are mainly elliptical with apertures of 0.1–0.3 μm, and some pores are irregular (Figs. 7(B1) and 7(B2)). The dolomite dissolution pores are mainly elliptical with apertures of 0.3–1 μm (Figs. 7(B3) and 7(B4)). The clay intergranular pores are mainly elliptical and sub-rounded with apertures of 1–3 μm (Fig. 7(B5)). Pyrite intergranular pores are developed with apertures of 30–100 nm (Fig. 7(B6)), and quartz inter-crystal pores are poorly developed (Fig. 7(B7)). The intragranular pores are developed in the organic band with an aperture of 50–200 nm and the number of organic pores is obviously greater than that of sample A with a TOC of 1.02% (Figs. 7(B8) and 7(B9)). The microfractures are mainly distributed inside the calcite and at the boundary between the organic band and inorganic minerals (Figs. 7(B9) and 7(B10)). By comparing the microscopic pores in the upper and middle $\epsilon_1 n^2$, the calcite dissolution pores, clay minerals intergranular pores and organic pores are the three main pore types, which are both developed in the two samples. Additionally, the types of micropores are clearly related to the mineral compositions, and more dolomite dissolution pores are found in sample B in the middle $\epsilon_1 n^2$ because of the much higher dolomite content. Finally, TOC has a strong influence on the micropore type. The organic micropores, microfractures, and pyrite intergranular pores are more developed in sample B than in sample A due to the higher TOC value.

4.3.5 Gas content

Taking well ZD2 as an example, the vertical variation in the gas content was analyzed (Fig. 2). The V_L of the three samples shows that the sample in the lower of $\epsilon_1 n^2$ has the highest gas content. The V_D ranges from 0.14 to 2.52 m^3/t, and the average value of the $\epsilon_1 n^1$, $\epsilon_1 n^2$ and $\epsilon_1 n^3$ are 0.80, 1.20 and 0.21 m^3/t, respectively. The total gas content (V_T) is consist of V_D, V_R, and the lost gas content. The curve of the V_T is similar to that of the V_D. In general, the gas content first shows a trend of slow increase with burial

depth, reaches a peak value at the bottom of the $\epsilon_1 n^2$, and finally decreases rapidly at the top of the $\epsilon_1 n^1$.

Horizontally, the average value of the V_D ranges from 0 to 2.05 m^3/t in the study area according to the sample tests of 16 wells (Table 2). The results show that the gas content is poor in most wells with V_D values less than 0.1 m^3/t, and wells with V_D values greater than 1.0 m^3/t are distributed only southeast of the Huangling anticline (B8).

5 Discussion

5.1 Factors influencing the shale gas content vertically

Taking the ZD2 well as an example, the factors that influence the shale gas content vertically were analyzed. The results show that the gas content has a positive linear correlation with TOC and the quartz content (Fig. 8(a) and

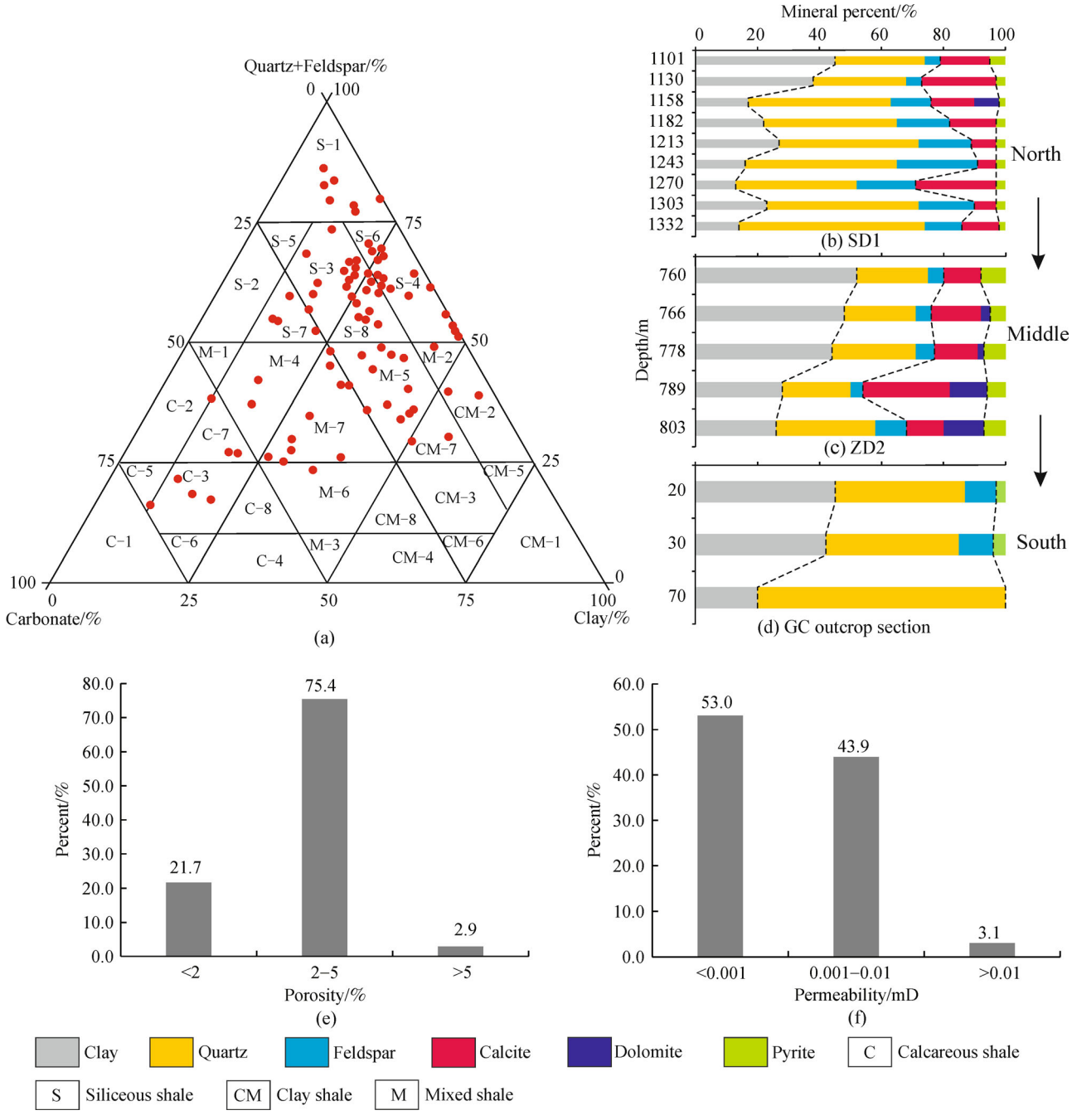

Fig. 6 Statistical characteristics of mineral content, porosity and permeability of organic-rich Shale of the $\epsilon_1 n^2$ in western Hubei. (a) Mineral composition in organic-rich Shale of the $\epsilon_1 n^2$; (b) mineral composition of well SD1 in deep shelf environment with argillaceous siltstone; (c) mineral composition of well ZD2 in deep shelf environment with carbonaceous shale; (d) mineral composition of GC stratigraphic outcrop of Hefeng county in deep shelf environment with carbonaceous siliceous; (e) porosity classification of organic-rich shale of the $\epsilon_1 n^2$ in western Hubei; (f) permeability classification of organic-rich shale of $\epsilon_1 n^2$ in western Hubei.

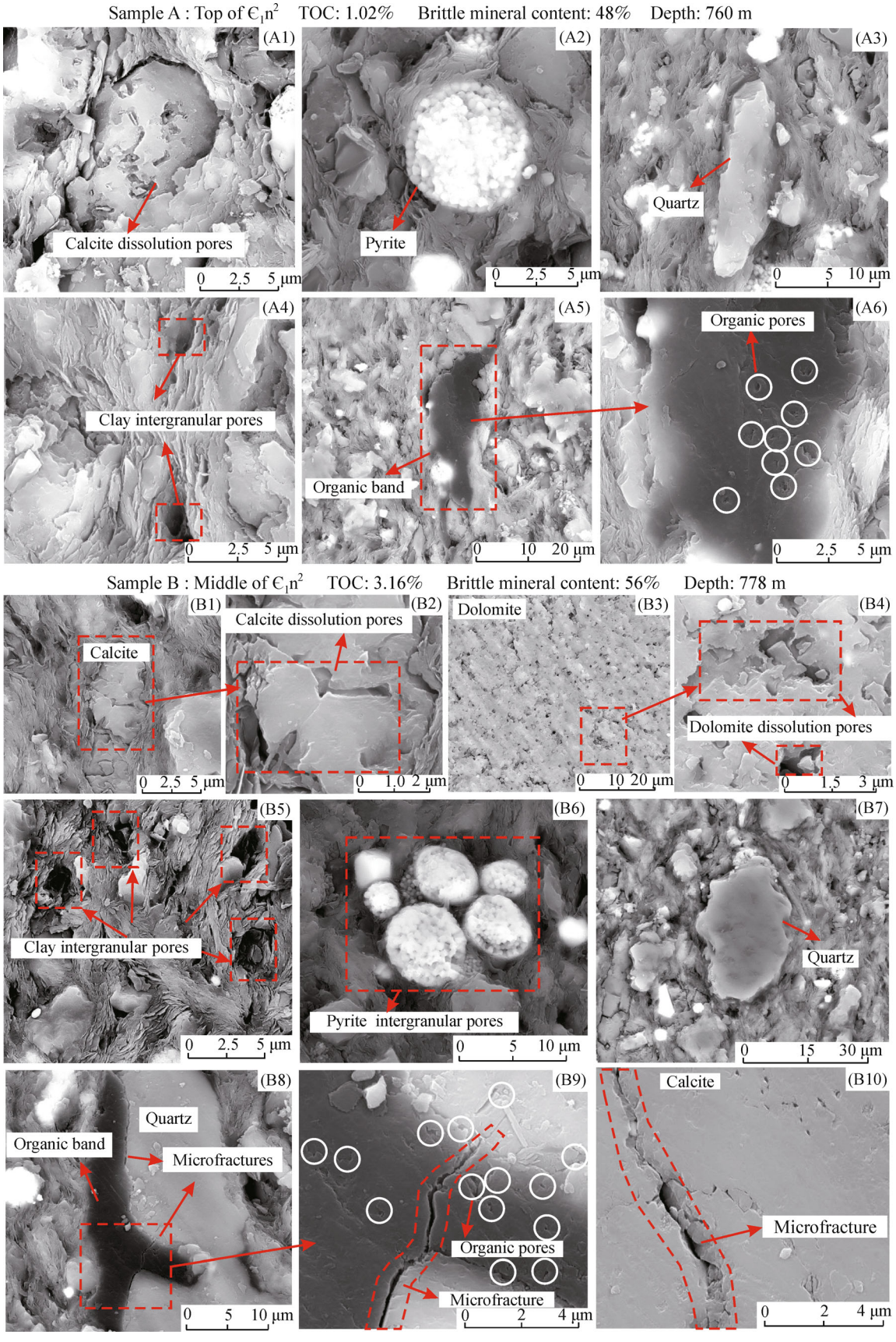

Fig. 7 Microscopic pores structure characteristic of the samples from well ZD2 of the $\epsilon_1 n^2$ obtained by argon ion polishing scanning electron microscopy. (A1) Calcite dissolution pores of Sample A; (A2) pyrite in Sample A; (A3) quartz in Sample A; (A4) clay intergranular pores in Sample A; (A5) organic band in Sample A; (A6) organic pores: the partial enlarged image of A5; (B1) calcite in Sample B; (B2) calcite dissolution pores: the partial enlarged image of B1; (B3) dolomite in Sample B; (B4) dolomite dissolution pores: the partial enlarged image of B3; (B5) clay intergranular pores of Sample B; (B6) pyrite intergranular pores of Sample B; (B7) quartz in Sample B; (B8) organic band in Sample B; (B9) microfractures: the partial enlarged image of B8; (B10) microfractures in calcite.

Table 2 Comprehensive data table of gas content of organic–rich shale of the $\epsilon_1 n^2$ in western Hubei

Wells	Depth/m	TOC/%	R_o/%	Porosity/%	Permeability/mD	Clay/%	Quartz/%	Carbonate/%	V_D/(m^3·t^{-1})	V_T/(m^3·t^{-1})
XD1	550.1	1.20 (1)	1.92(1)	2.6(1)	0.00085(1)	43(1)	/	/	0.00 (1)	/
YD3	837	/	/	/	/	/	/	/	0.00 (1)	0.02 (1)
SD1	1366	0.20–5.75/ 2.06 (107)	2.92–3.55/ 3.16(5)	0.1–2.2/ 0.52(40)	0.0014–0.0035/ 0.0024(14)	6–55/26.1(46)	2–77/ 39.8(46)	2–90/ 18.3(6)	0.01–0.48/ 0.10 (58)	/
HD1	1852	2.08 (1)	3.22(1)	/	/	/	/	/	0.05 (1)	0.13 (1)
YD2	1728	0.52–5.96/ 2.26 (29)	2.25–2.35/ 2.31(3)	/	/	/	/	/	0.1–3.65/ 1.54 (29)	0.18–5.58/ 2.24 (29)
YY1	1872	0.98–7.4/ 3.65 (29)	2.26–2.37/ 2.35(29)	/	/	/	/	/	0.58–5.48/ 2.05 (29)	/
ZD1	358.4	0.53–8.72/ 3.14 (17)	1.43–1.79/ 1.61(6)	1.18–3.46/ 2.26/(6)	0.00061–0.00327/ 0.00179(6)	15–50/26(6)	18–48/ 31(6)	8–39/ 26.2(6)	0.001–0.57/ 0.15 (20)	0.234–1.047/ 0.593 (20)
ZD2	804.9	0.41–5.02/ 2.61 (10)	2.05–2.59/ 2.34(10)	1.95–3.72/ 2.71(5)	0.00017–0.00186/ 0.00085(5)	26–52/39.6(5)	22–32/ 25.4(5)	16–43/ 25.8(6)	0.42–2.52/ 1.22 (16)	0.78–4.44/ 2.27 (16)
Y1	3070	1.0–5.2/ 2.2 (280)	2.70(1)	1.32–6.26/ 3.68(16)	0.001–1.15/ 0.36(14)	15.4(1)	/	/	0.14–2.26/ 1.05 (27)	0.30–3.60/ 2.10 (27)
YD1	1213.5	3.37 (3)	/	/	/	/	/	/	0.05 (3)	0.12 (3)
CD1	390.2	1.2–12.49/ 5.36 (35)	2.21–2.56/ 2.39(3)	1.2–4.35/ 2.76(18)	0.00025–0.00348/ 0.00105(17)	6–41/25.4	23–76/44.9	5–39/ 14.1(13)	0.03–0.17/ 0.08 (30)	0.13–0.71/ 0.32 (30)
ND1	754	1.46–14.44/ 6.88 (33)	2.61–2.72/ 2.64(3)	0.27–6.76/ 1.61(9)	0.0007–0.65/ 0.0786(9)	7.9–32/15.6(10)	24.2–74.2/ 40.9(10)	10–64/ 40.5(10)	0.03–0.15/ 0.08 (20)	0.24–1.30/ 0.67 (20)
YD4	1334	/	/	/	/	/	/	/	0.06–3.13/ 1.55 (12)	/
EY1	3945	1.5–6.2/ 5.1 (12)	/	/	/	/	/	/	0.1–0.4/ 0.26 (12)	/
WD1	1602	4.10 (1)	3.50(1)	/	/	/	/	/	0.02 (1)	/
X1	1406	/	/	/	/	/	/	/	0.00 (1)	/

Notes: The value consists of minimum value, maximum value, average value and the number of samples, "/" indicates that the data has not been collected. "V_D" is field canister desorption gas content; "V_T" is the total gas content.

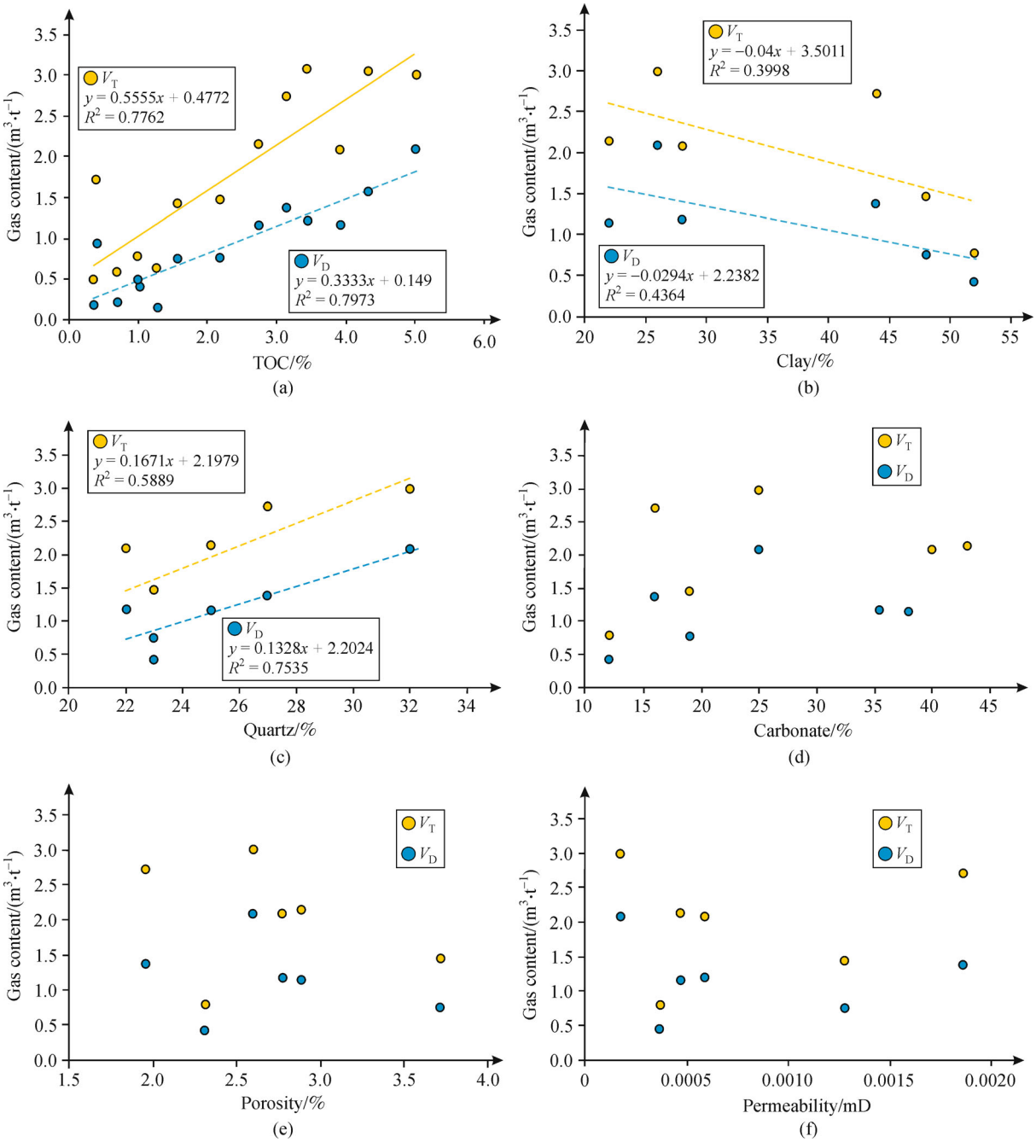

Fig. 8 Factors influencing the shale gas content vertically of the $\epsilon_1 n^2$ in ZD2 well. (a) The correlation between gas content and TOC; (b) The correlation between gas content and clay content; (c) the correlation between gas content and quartz content; (d) the correlation between gas content and carbonate content; (e) the correlation between gas content and porosity; (f) the correlation between gas content and permeability.

8(c)). The clay content (Fig. 8(b)), carbonate content (Fig. 8(d)), porosity (Fig. 8(e)), and permeability (Fig. 8(f)) have no obvious correlations with the gas content. Organic matter content is an important index to evaluate shale reservoir quality. Organic matter is not only the source of shale gas but also provides storage space for shale gas (Wang et al., 2009; Tan et al., 2014). The good linear correlation between TOC and gas content can be explained by the correlation between TOC and the specific surface area, total pore volume and number of organic pores in shale reservoirs. TOC has a positive correlation with the specific surface area and total pore volume and with the R^2 values of 0.8504 and 0.5597, respectively (Fig. 9). Additionally, when comparing sample A with a TOC

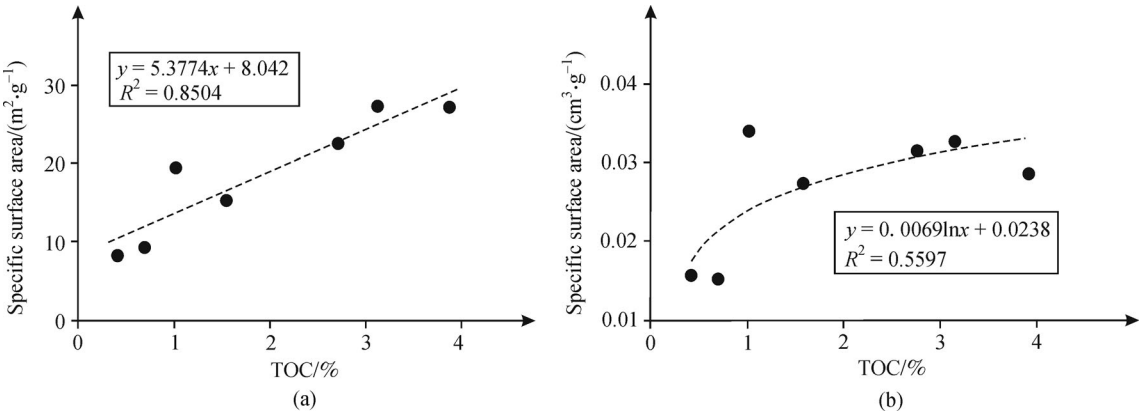

Fig. 9 The correlation between specific surface areas, and pore volume with TOC of the samples of the $\epsilon_1 n^2$ from the wells ZD1 and ZD2. (a) The correlation between specific surface areas and TOC; (b) the correlation between total pore volume and TOC.

content of 1.02% and sample B with a TOC content of 3.16%, the samples with a TOC content of 3.16% had more organic pores (Figs. 7(A6) and 7(B9)).

Mineral composition in shale can directly control the development of micropores (Gasparik et al., 2012; Gou and Xu, 2019; Tang et al., 2019); thus, it can influence the gas content (Lu et al., 1995; Ji et al., 2012). In this paper, the gas content has a better correlation with quartz than clay and carbonate minerals. Previous studies have shown that the quartz content has a better relationship with the gas content because a high quartz content can provide a large part of the pore volume (Tang et al., 2016). However, microscopic observation by SEM showed that the micropore of quartz barely develop (Figs. 7(A3) and 7(B7)). Further research shows that, on the one hand, the high quartz content is not only conducive to the formation of microfractures but also has good compaction resistance, which can prevent the pores from being destroyed and thus increase the total pore volume of shale; on the other hand, the study of 12 samples from the wells ZD1 and ZD2 shows that the quartz content has a clear positive correlation with the TOC content with an R^2 of 0.5517, and both the clay and carbonate content have no clear correlation with the TOC content (Fig. 10). Since the quartz intragranular pores are barely developed in the microscopic pores (Figs. 7(A3) and 7(B7)), the quartz content correlates well with the gas content, which maybe caused by two possible reasons. One possible reason is that quartz and organic matter are coupled symbioses, which leads to a good positive correlation of quartz with TOC (Fig. 10). The other reason is that a high quartz content is conducive to the formation of microfractures, which can improve the permeability of the $\epsilon_1 n^2$ in the well ZD2 (Fig. 7(B8)).

5.2 Influencing factors of shale gas content horizontally

Based on the results, the gas content has a good vertical correlation with the TOC and quartz mineral content. However, the gas content has no obvious horizontal correlation with TOC and quartz mineral content by using the data of wells ZD1, ZD2, SD1, and ND1 wells in the deep shelf (Figs. 11(a) and 11(b)). Therefore, the gas content is obviously horizontally affected by the other

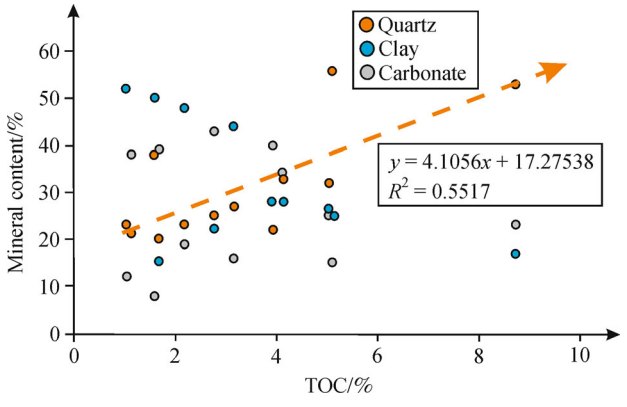

Fig. 10 The correlation between mineral composition and TOC of the samples of the $\epsilon_1 n^2$ from the wells ZD1 and ZD2.

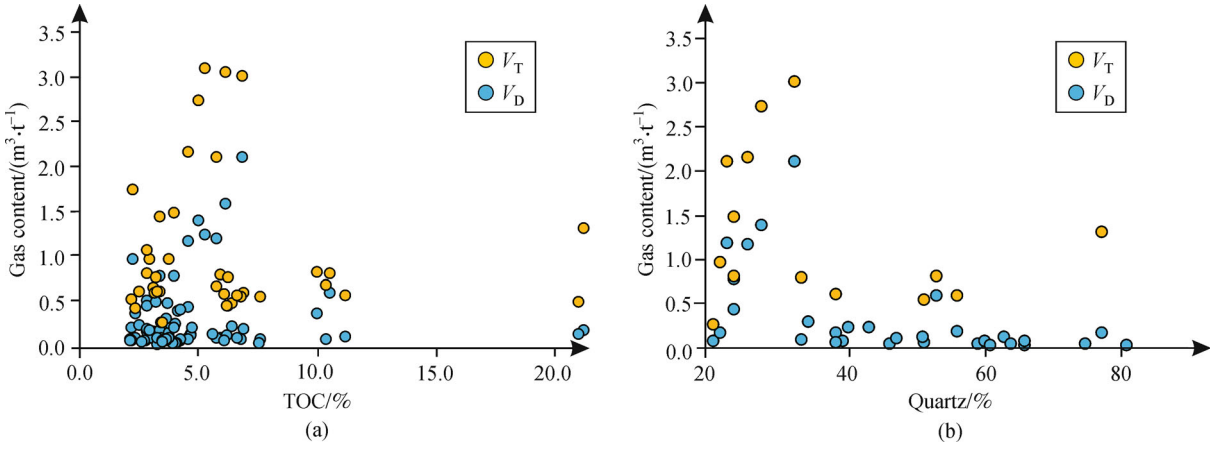

Fig. 11 The horizontal correlation between gas content with TOC, and Quartz content of the $\epsilon_1 n^2$ in western Hubei. (a) The horizontal correlation between gas content with TOC of the $\epsilon_1 n^2$; (b) the horizontal correlation between gas content with quartz content of the $\epsilon_1 n^2$.

factors. To clarify the factors that influence the gas content horizontally, the factors that influence the gas content were studied in the following sections, such as sedimentary facies, structural style, fault and fracture characteristics, thermal evolution degree, stratigraphic unconformity and burial depth.

5.2.1 Sedimentary influences on the gas content

The sedimentary environment controls the formation of organic-rich shale and determines the quality of shale gas reservoirs (Algeo and Tribovillard, 2009; Liu et al., 2015; Zhao et al., 2019). The relationship between sedimentary facies and thickness, TOC and gas content was studied based on the 36 thickness data points, 33 TOC data points and 16 V_D data points (Figs. 3(a), 3(b), and 3(c)). The shale thickness is highest, with a value of 186.3 m, in the deep shelf environment with argillaceous siltstone, followed by the deep shelf environment with carbonaceous siliceous rock, the deep shelf environment with carbonaceous shale, and the carbonate shallow shelf and submarine uplift environments with the thickness of 128.8 m, 114.7 m, 42.5 m, and 7.5 m, respectively (Fig. 3(b)). The TOC is highest in the deep shelf environment with carbonaceous siliceous rock, with an average value of 4.0%, followed by the deep shelf environment with carbonaceous shale, the deep shelf with the argillaceous siltstone, and the shallow carbonate shelf and submarine uplift environments with average values of 3.8%, 2.2%, 1.5%, and 1.2%, respectively (Fig. 3(c)). The statistical results show that the deep shelves with carbonaceous shale and carbonaceous siliceous rock with higher TOC contents are much more beneficial to the accumulation of shale gas. The deep shelf with argillaceous siltstone has the largest shale thickness. However, its TOC content is much lower than that of deep shelf with carbonaceous shale and carbonaceous siliceous rock.

The sedimentary facies influences the gas content of drilling wells by controlling the thickness and TOC of the shale. The results show that the V_D is 0.0 m^3/t in both the XD1 and YD3 wells, which are located in the submarine uplift because of the low values of TOC and thickness. The V_D is greater than 1.0 m^3/t in the ZD2, YD2, YY1, and YD4 wells, which are located in the deep shelf because of the larger values of TOC and thickness (Fig. 3(a)). However, the gas content is very low in some wells located in the deep shelf with large TOC contents and thicknesses, such as EY1, SD1, HD1, CD1, WD1, X1, YD1, ND1, and ZD1. The gas content is influenced not only by sedimentary facies, but also by other factors. Therefore, the influence of structural style, fault properties and other factors on the gas content is thoroughly discussed in the following sections.

5.2.2 Structural type influencing the gas content

The degree of fold deformation and fracture development is generally different in tectonic belts, and a weak tectonic zone is favorable for the preservation of shale gas (Wang et al., 2016). A total of 14 wells were used to analyze the impact of structural type on gas content in the study area (Fig. 12). The results show that areas with wide and gentle folds and that are also away from large normal faults are beneficial for shale gas accumulation, such as wells ZD2, YD2, YD4, YY1, and Y1 with V_D values of 1.22, 1.54, 1.55, 2.05, and 1.05 m^3/t, respectively (Figs. 12(c), 12(g), and 12(i)). In contrast, the gas content is poor in the cores of anticlines, such as in wells X1, CD1, and YD1 (Figs. 12(a), 12(b), and 12(f)). However, the gas content is poor in some survey wells with wide and gentle folds, such as in wells EY1, WD1, ND1, ZD1, HD1, and SD1. Therefore, the reason for the poor gas content is analyzed in detail in the following sections.

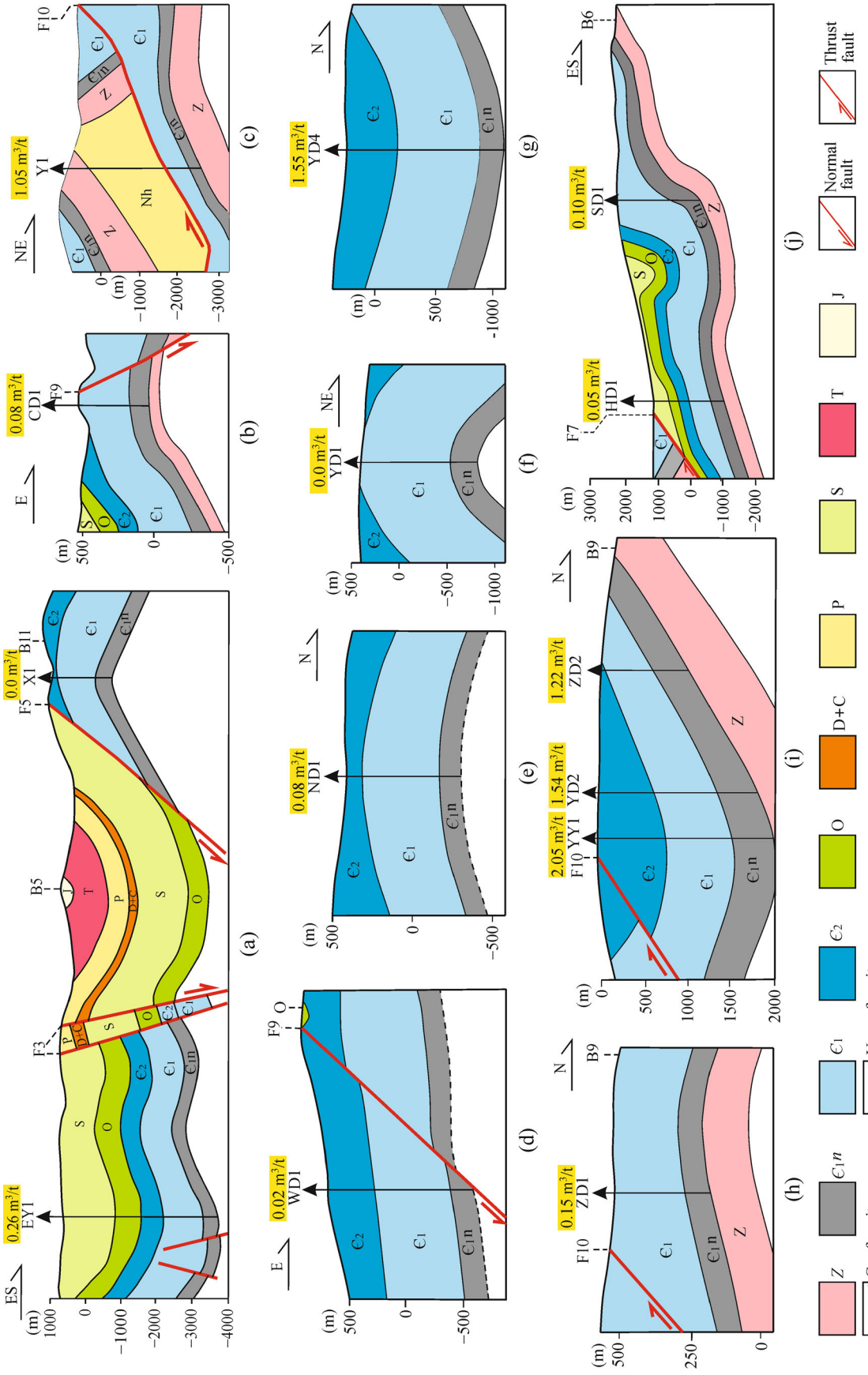

Fig. 12 Tectonic position of 14 wells in western Hubei. (a) tectonic position of the EY1 and X1 wells; (b) tectonic position of the CD1 well; (c) tectonic position of the Y1 well; (d) tectonic position of the WD1 well; (e) tectonic position of the ND1 well; (f) tectonic position of the YD1 well; (g) tectonic position of the YD4 well; (h) tectonic position of the ZD1 well; (i) tectonic position of the YY1, YD2, and ZD2 wells; (j) tectonic position of the HD1 and SD1 wells.

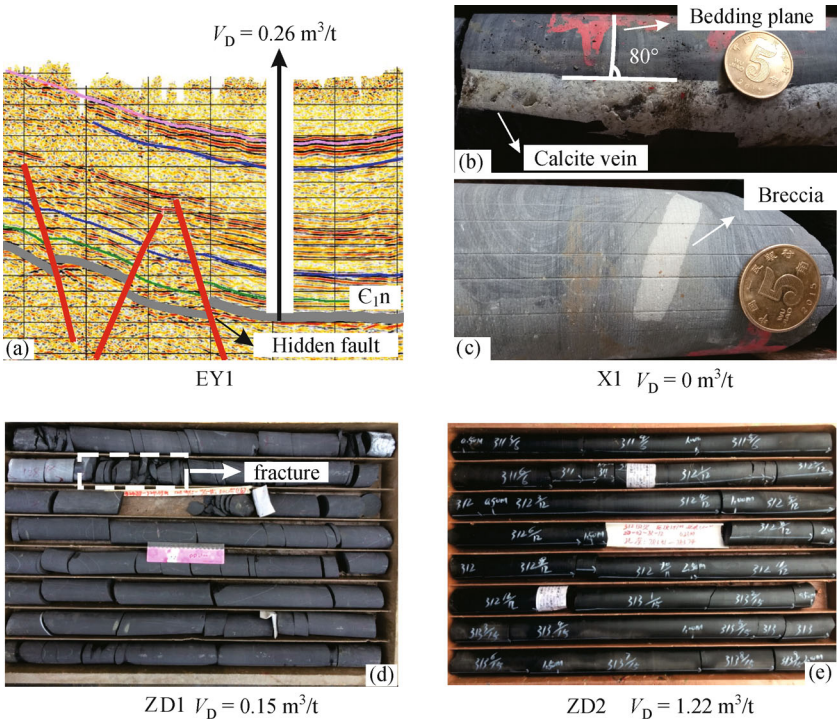

Fig. 13 The correlation between the fracture characteristics and gas-bearing strata of the ϵ_1n in wells EY1, X1, and ZD2. (a) The hidden faults in seismic profile of the EY1 well; (b) high Angle calcite vein in the X1 well; (c) the fractures locally developed in the ZD1 well; (d) the fractures barely developed in the ZD2 well.

5.2.3 The influence of faults and fractures on the gas content

Shale gas can be lost when normal faults cut through shales and their roofs and floors. When high-angle fractures develop, they are not conducive to shale gas preservation (Wang et al., 2016). The CD1 and WD1 wells are located near the Xiannvshan normal fault (F9), and the up-dip direction of the shale formation communicates with the fault; thus, shale gas is easily escapes, resulting in very low gas contents of 0.08 and 0.02 m³/t, respectively (Figs. 12(b) and 12(d)).

Specifically, the EY1 well is located in the core of a secondary syncline in the Zhongyang anticline belt (B4), and its structural position is relatively favorable. However, the well location is close to the hidden normal fault underground, which results in a low gas content of 0.26 m³/t (Figs. 12(a) and 13(a)). The correlation between the fracture characteristics and gas-bearing strata was studied by observing the fractures in the cores of wells X1, ZD1, and ZD2. The results show that breccia and calcite veins developed in the X1 well. The calcite vein is approximately 1 cm wide and presents an 80° angle to the shale bedding face. The development of high-angle fractures results in no gas in the well (Figs. 13(b) and 13(c)). There is some gas in wells ZD1 and ZD2 with V_D values of 0.15 and 1.22 m³/t, respectively, because fractures develop poorly in the core, especially in the core of well ZD2, which is very intact (Figs. 13(d) and 13(e)). Nine wells near the normal Xiannvshan fault were chosen to analyze the correlation between the V_D and the distance from the normal fault to the wells. The selected wells are all in the deep shelf and are away from the core of the anticline. The results show that the V_D has an obvious positive linear correlation with the distance from the Xiannvshan fault with a correlation coefficient of 0.6204. The V_D value is less than 0.5 m³/t when the distance is less than 5 km (Fig. 14).

5.2.4 Thermal evolution degree influencing on the gas content

The degree of thermal evolution of shale is the main factor controlling the micropore structure. After shale reaches the over-mature state, its specific surface area and pore volume decrease sharply with increasing R_o. Meanwhile, the contents of smectite and illite with larger specific surface areas decreased, and the chlorite with small specific surface areas increased (Liang et al., 2014). The correlation between the gas content and R_o shows that when R_o is greater than 3.0%, the V_D is less than 0.1 m³/t. Additionally, the value of R_o ranges from 2.0% to 2.5% in wells with high gas contents, such as in wells YD2, YY1, and ZD2 (Fig. 15(a)). Although the SD1 and HD1

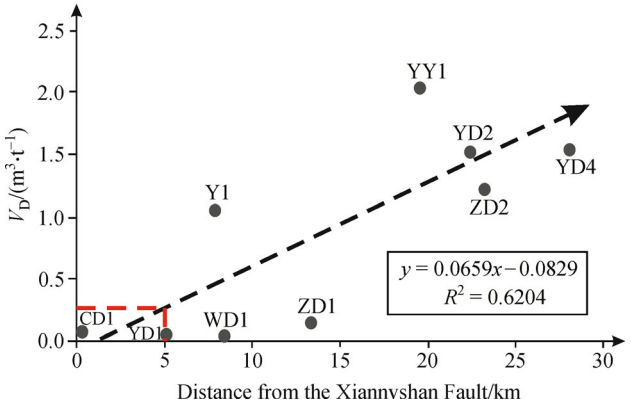

Fig. 14 The correlation between the V_D and the distance from Xiannvshan Fault (F9) to the nine wells in western Hubei.

wells are located in the deep shelf with large shale thicknesses and high TOC contents, the gas content is very low in the two wells. The reason is that the high R_o value of the two wells are influenced by the Yangri Fault (F7). It is a large thrust fault fracture with strong seismic activity and a hot spring distribution along the fault, and the $\epsilon_1 n$ shale is heated by the tectonic movement. Therefore, shale thermal evolution is relatively high, which results in a smaller specific surface area and pore volume, and thus, the gas content is very low in both SD1 and HD1 wells.

When comparing the SD1 with the ZD2 well, the R_o values of ZD2 are relatively low with higher contents of smectite and illite and lower contents of chlorite (Fig. 15(b)), which result in a larger specific surface areas and pore volume. Experimental tests show that the average porosity in well ZD2 is 2.71%, which is much higher than the value of 0.52% in the SD1. Therefore, compared with the ZD2, the low specific surface areas and porosity due to higher thermal evolution are the main reasons for the low gas content in the SD1 well.

5.2.5 Influences of the roof and floor sealing capacity on the gas content

The sealing property of organic-rich shale can be divided into macro-sealing and Micro-sealing. Macro-sealing refers to the lithology, thickness and transverse distribution stability of the target, top and bottom layers. Micro-sealing includes shale porosity, permeability and brittle mineral content (Lou et al., 2011; Pan et al., 2014). The analysis indicates that the $\epsilon_1 n^2$ shale gas target layer has good self-sealing properties and an average thickness of 133.9 m. The average thicknesses of the roofs of $\epsilon_1 n^3$ and $\epsilon_1 sp$ organic-rich shales are 83.2 m and 276.4 m, respectively. The average thicknesses of the floors of the $\epsilon_1 n^1$ and $Z_2 d$ organic-rich shales are 17.2 m and 221.7 m, respectively (Fig. 16(a)). Additionally, the $\epsilon_1 n^3$ has a better sealing capacity than the $\epsilon_1 n^1$ due to its low brittle mineral content (Fig. 16(b)). In particular, there is an important discovery in this study according to the 21 data points of wells and stratigraphic sections. The $\epsilon_1 n^1$ is distributed only in the deep shelf of the central and northern parts of the study area (Fig. 16(c)) and is absent in the eastern and southern parts of the study area, where the $Z_2 d$ unconformably contacts the $\epsilon_1 n^2$ stratigraphically. For example, the $\epsilon_1 n^1$ is developed in the core of the ZD2 well with a thickness of 12.6 m (Fig. 16(d)), while it is absent in the core of the ND1 well (Fig. 16(e)). The unconformity boundary is very clear in Hefeng county, and the shale of the $\epsilon_1 n^2$ is overlain on the dolomite of the Dengying Formation ($Z_2 d$) with weathered crust in the middle (Fig. 16(f)). The results show that, first, the unconformity boundary is the main reason for the poor gas content in the wells located in the southern part of the boundary, such as wells ND1 and WD1 wells. In addition, the existence of the unconformity boundary leads to the loss of shale gas in the southern and eastern parts of the study area, which is not conducive to the preservation of shale gas.

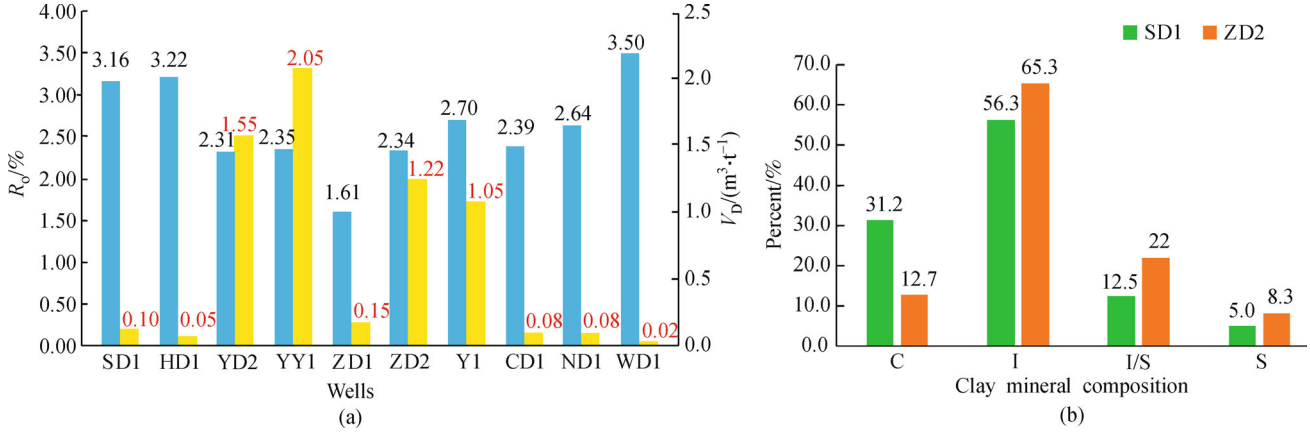

Fig. 15 The correlation between gas content and *Ro* of the $\epsilon_1 n^2$. (a) The correlation between V_D and R_o; (b) Comparison of clay mineral types between the wells ZD2 and SD1. Notation: "C" is chlorite; "I" is illite; "S" is smectite.

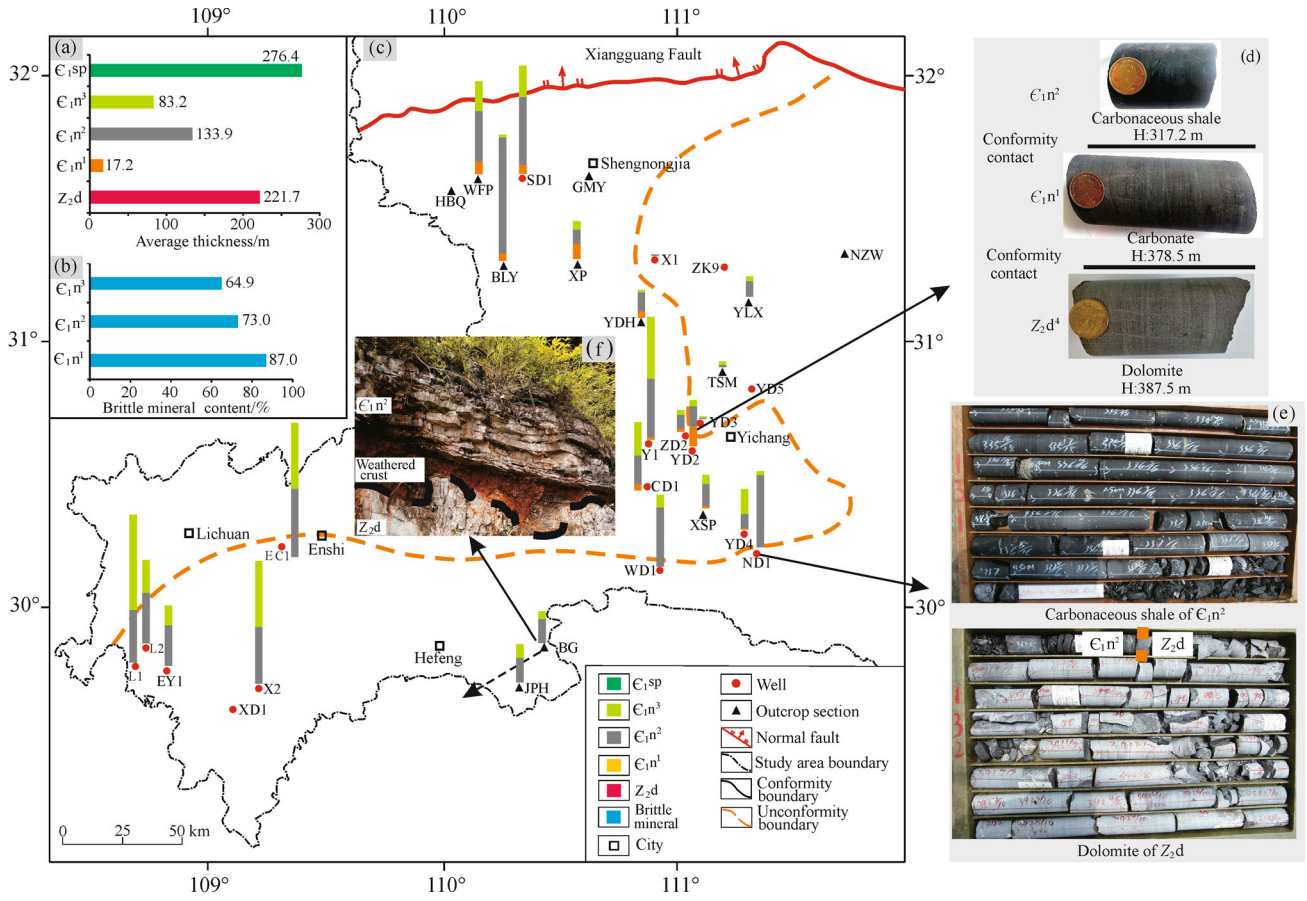

Fig. 16 Influences of the roof and floor sealing capacity on the shale gas preservation: (a) the average thicknesses of $\in_1$sp, $\in_1$n, and Z_2d formations; (b) the brittle mineral content of $\in_1n^1$, $\in_1n^2$, and $\in_1n^3$; (c) the thickness distribution of $\in_1n^1$, $\in_1n^2$ and $\in_1n^3$ in western Hubei; (d) $\in_1n^1$ conformably contacts Z_2d of the ZD2 well; (e) $\in_1n^2$ unconformably contacts the Z_2d of the ND1 well; (f) $\in_1n^2$ unconformably contacts the Z_2d of BG stratigraphic section.

5.2.6 Influencing of burial depth on the gas content

The burial depth is very important for the formation of shale gas reservoirs. Shale gas reservoirs are susceptible to infiltrating atmospheric water, which results in gas loss when the burial depth is too shallow (Si et al., 2016). The correlation was studied between the V_D and burial depth of the ZD1, ZD2, YD4, YD2, and YY1 wells. These five wells are located on the deep shelf facies in the southeastern side of the Huangling anticline (B8), far from the large regional normal Xiannvshan Fault (F9); thus, the burial depth plays a major role in the gas content.

The results show that the average burial depths of $\in_1n^2$ in ZD1, ZD2, YD4, YD2, and YY1 are 300.8, 781.8, 1292.6, 1693.7, and 1857.5 m, respectively, with average V_D value of 0.16, 1.22, 1.69, 1.9, and 1.84 m^3/t, respectively. Therefore, the V_D increases with burial depth, and there is an exponential correlation between gas content and burial depth with a correlation coefficient of 0.5799. Additionally, when the burial depth is less than 500 m, the average value of V_D is lower than 0.5 m^3/t, and when the burial depth exceeds 500 m, the influence of the burial depth on the gas content gradually decreases, especially when the burial depth is greater than 1500 m, and the influence of the burial depth on the gas content is negligible (Fig. 17(a)).

The burial depth affects not only the gas content but also the gas composition. The correlation between methane content and burial depth was studied for wells ZD1 and ZD2. The results show that the methane content increases with burial depth for both wells (Figs. 17(b) and 17(c)). In particular, the methane content of the ZD1 well increases obviously when the burial depth is greater than 300 m (Fig. 17(b)). Thus, the depth of 300 m may be the groundwater boundary between the free alteration zone and the stagnation zone.

Based on the correlation analysis between the gas content and sedimentary facies distribution, structural style, fault and fracture development characteristics, degree of thermal evolution, regional unconformity boundary and burial depth, wells with low gas contents are generally affected by the combination of two or more factors. Additionally, the combination of structural styles, fault and fracture development, and the distribution of the regional unconformity boundary are the three most

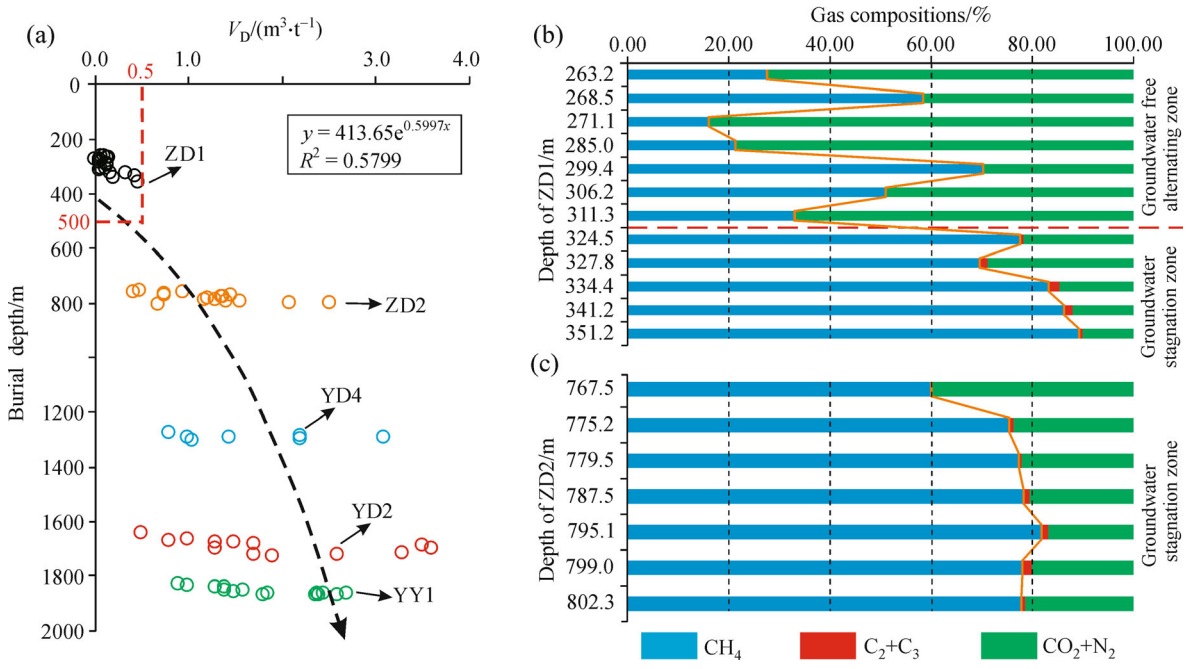

Fig. 17 Influences of the burial depth on the shale gas content and compositions. (a) The correlation between the V_D and burial depth; (b) the correlation between the gas compositions and burial depth of the ZD1 well; (c) the correlation between the gas compositions and burial depth of the ZD2 well.

important factors affecting the gas content. The areas with high gas content must meet the following conditions: deep shelf environment, $\epsilon_1 n^1$ is present, wide and gentle syncline, away from large normal faults greater than 5 km, the moderate thermal evolution and the burial depth of greater than 500 m.

5.3 Favorable block evaluation

According to these results and the Technical Specification for Calculation and Evaluation of Shale Gas Resources/ Reserves issued by the Ministry of Natural Resources (DZ/ T 0254-2014), the evaluation index system of favorable shale gas area in western Hubei was established, and the favorable blocks were selected.

This study shows that the selected favorable areas must meet the following nine conditions: 1) continuous distribution area≥50 km^2; 2) thickness of organic-rich shale of more than 20 m; 3) TOC≥1.0%; 4) V_D≥1.0 m^3/t; 5) wide and gentle fold belt; 6) away from normal fault greater than 5 km, low fracture density, and high-angle fractures that are not developed in the core; 7) good sealing properties of the roof and floor, and no stratigraphic unconformity; 8) R_o distribution in the range of 1.3%–3.0%; (9) burial depth≥500 m.

According to the above nine conditions, three favorable areas of western Hubei are determined by overlapping the buried depth, shale thickness, TOC and R_o contour maps of organic-rich shale. The favorable areas are mainly distributed in the southern Huangling anticline (B8) and northern Xiannvshan fault (F9), which contain the YD2–ZD2 well block, Y1 well block and YD4 well block (Fig. 18).

6 Conclusions

Based on systematic research on the geological controls of shale gas accumulation and the enrichment mechanism of the lower Cambrian Niutitang Formation, the conclusions are as follows:

1) The Niutitang Formation can be vertically divided into three sections, and the $\epsilon_1 n^2$ is mainly a shale gas reservoir. The deep shelf facies is the main sedimentary facies and can be divided into three lithofacies: argillaceous siltstone, carbonaceous shale and carbonaceous siliceous rock.

2) There are two main shale deposits with shale thicknesses greater than 200 m. Vertically, the TOC shows gentle growth trends until the depth reaches the bottom of the $\epsilon_1 n^2$ and then decreases rapidly in the $\epsilon_1 n^1$. Horizontally, the TOC is mainly distributed from 2% to 4%. Siliceous shale is the main lithofacies, and the average brittle mineral content is high. The reservoir has low porosity and ultra-low permeability. Calcite dissolution and clay intergranular and organic pores are the main pore types and micropores types are clearly related to the mineral and TOC contents.

3) Vertically, the gas content is mainly affected by TOC. Since the quartz intragranular pores are barely developed

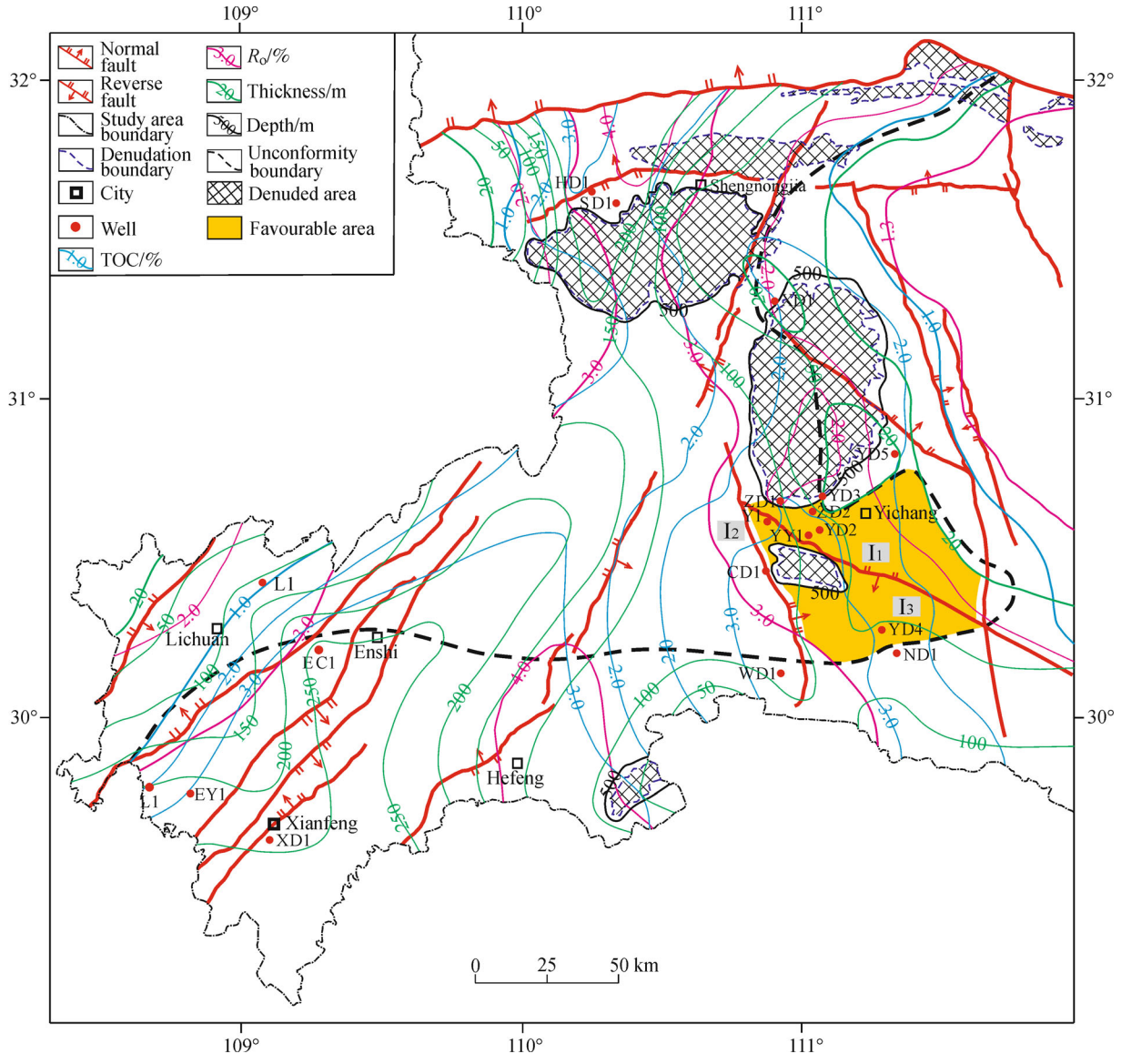

Fig. 18 Comprehensive evaluation of shale gas favorable block of the $\epsilon_1 n^2$ in western Hubei.

in the microscopic pores, the good correlation of the quartz content with the gas content may be caused by the coupled symbioses of the quartz and organic matter, which leads to the good positive correlation of the quartz with TOC; the high quartz content is conducive to the formation of microfractures that improve the permeability.

4) Horizontally, the gas content has no obvious correlation with TOC and quartz mineral content and changes greatly in different tectonic units, with high gas contents distributed only southeast of the Huangling anticline. The combination of structural styles, fault and fracture development, and the distribution of the regional unconformity boundary between the upper Sinian Dengying Formation (Z_2d) and the $\epsilon_1 n^2$ are the three most important factors affecting the gas content.

5) The favorable areas must meet the following conditions: deep shelf environment, $\epsilon_1 n^1$ is present, wide and gentle syncline, away from large normal faults greater than 5 km, moderate thermal evolution and burial depth of greater than 500 m, this includes the YD2–ZD2 well block, Y1 well block and YD4 well block, which are distributed in the southern Huangling anticline and northern Xiannvshan Fault.

Acknowledgements This work is supported by the Scientific Research project of Department of Natural Resources of Hubei Province (No. ZRZY2020KJ10) and Hubei Geological Bureau (No. KJ2019-3); the Shale Gas Geological Survey Projects of Department of Natural Resources of Hubei Province (Nos. HBCZ-17060223-170397 and DTCG-190409); We also thank the funds provided by Youth Foundation of the Northeast Petroleum University (No. 2019QNL-21); Opening Fund of the Coal Reservoir Laboratory of National Engineering Research Center of CBM Development & Utilization, China University of Geosciences (Beijing) (No. 2019MCQ02001). We would like to thank laboratory staff who helped

with the experiments. We would like to also thank Sinopec Jianghan Oilfield Research Institute of Exploration and Development and Wuhan Center of China Geological Survey to provide the drilling well data. Careful reviews and constructive suggestions of the manuscript by anonymous reviewers are also greatly appreciated.

References

Algeo T J, Tribovillard N (2009). Environmental analysis of paleoceanographic systems based on molybdenum-uranium covariation. Chem Geol, 268(3–4): 211–225

Ambrose R J, Hartman R C, Campos M D, Akkutlu I Y, Sondergeld C (2010). New pore-scale considerations for shale gas in place calculations. Society of Petroleum Engineers Unconventional Gas Conference. Pittsburgh, Pennsylvania, USA, SPE Paper 131772

Aringhieri R (2004). Nanoporosity characteristics of some natural clay minerals and soils. Clays Clay Miner, 52(6): 700–704

Best M E, Katsube T J (1995). Shale permeability and its significance in hydrocarbon exploration. Leading Edge (Tulsa Okla), 14(3): 165–170

Bowker K A (2003). Recent developments of the Barnett Shale play, Fort Worth Basin. West Texas Geol Soc Bull, 42(6): 4–11

Bowker K A (2007). Barnett Shale gas production, Fort Worth Basin: issues and discussion. AAPG Bull, 91(4): 523–533

Chalmers G R L, Bustin R M (2008). Lower cretaceous gas shales in northeastern British Columbia. Part I: geological controls on methane sorption capacity. Bull Can Pet Geol, 56(1): 1–21

Chalmers G R, Bustin R M (2015). Porosity and pore size distribution of deeply-buried fine-grained rocks: influence of diagenetic and metamorphic processes on shale reservoir quality and exploration. J Unconvent Oil Gas Resour, 12: 134–142

Chalmers G R, Bustin R M, Power I M (2012). Characterization of gas shale pore systems by porosimetry, pycnometry surface area, and field emission scanning electron microscopy/transmission electron microscopy image analyses: examples from the Barnett, Woodford, Haynesville, Marcellus, and Doig units. AAPG Bull, 96(6): 1099–1119

Cheng A L, Huang W L (2004). Selective adsorption of hydrocarbon gases on clays and organic matter. Org Geochem, 35(4): 413–423

Clarkson C R, Solano N, Bustin R M, Bustin A M M, Chalmers G R L, He L, Melnichenko Y B, Radliński A P, Blach T P (2013). Pore structure characterization of North American shale gas reservoirs using USANS/SANS, gas adsorption, and mercury intrusion. Fuel, 103: 606–616

Curtis J B (2002). Fractured shale gas systems. AAPG Bull, 86(11): 1921–1938

Curtis M E, Cardott B J, Sondergeld C H, Rai C S (2012 a). Development of organic porosity in the Woodford Shale with increasing thermal maturity. Int J Coal Geol, 103: 26–31

Curtis M E, Sondergeld C H, Ambrose R J, Rai C S (2012 b). Microstructural investigation of gas shales in two and three dimensions using nanometer-scale resolution imaging. AAPG Bull, 96(4): 665–677

EIA (2011). World Shale Gas Resources: An Initial Assessment of 14 Regions Outside the United States. Washington DC: U.S. Department of Energy

Gasparik M, Ghanizadeh A, Bertier P, Gensterblum Y, Bouw S, Krooss B M (2012). High-pressure methane sorption isotherms of black shales from the Netherlands. Energy Fuels, 26(8): 4995–5004

Gou Q, Xu S (2019). Quantitative evaluation of free gas and adsorbed gas content of Wufeng-Longmaxi shales in the Jiaoshiba area, Sichuan Basin, China. Advan in Geo-Ener Resear, 3(3): 258–267

Guo T, Zhang H (2014). Formation and enrichment mode of Jiaoshiba shale gas field, Sichuan Basin. Pet Explor Dev, 41(1): 31–36

Hao F, Zou H Y, Lu Y C (2013). Mechanism of shale gas storage: implications for shale gas exploration in China. AAPG Bull, 97(8): 1325–1346

Huang J L, Zou C N, Li J Z, Dong D Z, Wang S J, Wang S Q, Cheng K M (2012). Shale gas generation and potential of the Lower Cambrian Qiongzhusi Formation in Southern Sichuan Basin, China. Pet Explor Dev, 39(1): 69–75

Huang Y R, Xiao Z H, Jiao P, Qin M Y, Yu Y, Wang X K, Cao T T (2018). Comparison of factors for shale gas accumulation in Niutitang formation wells in northwestern Hunan and its implications. J Centr South Univ (Sci & Tech), 49(9): 2240–2248

Hughes J D (2013). A reality check on the shale revolution. Nature, 494 (7437): 307–308

Jarvie D M, Hill R J, Ruble T E, Pollastro R M (2007). Unconventional shale-gas systems: the Mississippian Barnett Shale of north-central Texas as one model for thermogenic shale-gas assessment. AAPG Bull, 91(4): 475–499

Ji L M, Zhang T W, Milliken K L, Qu J L, Zhang X L (2012). Experimental investigation of main controls to methane adsorption in clay-rich rocks. Appl Geochem, 27(12): 2533–2545

Jin Z J, Nie H K, Liu Q Y, Zhao J, Jiang T (2018). Source and seal coupling mechanism for shale gas enrichment in upper Ordovician Wufeng Formation-Lower Silurian Longmaxi Formation in Sichuan Basin and its periphery. Mar Pet Geol, 97: 78–93

Li A, Ding W L, He J H, Dai P, Yin S, Xie F (2016). Investigation of pore structure and fractal characteristics of organic-rich shale reservoir: a case study of Lower Cambrian Qiongzhusi Formation in Malong block of eastern Yunnan Province, Southern China. Mar Pet Geol, 70: 46–57

Li A, Ding W L, Jiu K, Wang Z, Wang R Y, He J H (2018). Investigation of pore structure and fractal characteristics of marine shale reservoirs using NMR experiments and image analyses: a case study of Lower Cambrian Niutitang formation in northern Guizhou Province, South China. Mar Pet Geol, 89: 530–540

Li J Q, Lu S F, Zhang P F, Cai J C, Li W B, Wang S Y, Feng W J (2020). Estimation of gas-in-place content in coal and shale reservoirs: a process analysis method and its preliminary application. Fuel, 259: 1–10

Li Y, Yang J, Pan Z, Meng S, Wang K, Niu X (2019a). Unconventional natural gas accumulations in stacked deposits: a discussion of Upper Paleozoic coal-bearing strata in the east margin of the Ordos Basin, China. Acta Geol Sin, 93(1): 111–129

Li Y, Wang Z, Pan Z, Niu X, Yu Y, Meng S (2019b). Pore structure and its fractal dimensions of transitional shale: a cross section from east margin of the Ordos Basin, China. Fuel, 241: 417–431

Liang X, Zhang T S, Yang Y, Zhang Z, Gong Q S, Ye X, Zhang J H (2014). Microscopic pore structure and its controlling factors of overmature shale in the Lower Cambrian Qingzhusi Formation,

northern Yunnan and Guizhou province of China. Nat Gas Ind, 34: 18–26 (in Chinese)

Liu K, Ostadhassan M (2019). The impact of pore size distribution data presentation format on pore structure interpretation of shales. Advan in Geo-Ener Resear, 3(2): 187–197

Liu Z H, Zhuang X G, Teng G E, Xie X M, Yin L M, Bian L Z, Feng Q L, Algeo T J (2015). The Lower Cambrian Niutitang Formation at Yangtiao (Guizhou, SW China): organic matter enrichment, source rock potential, and hydrothermal influences. J Pet Geol, 38(4): 411–432

Lou Z H, Shang C J, Yao G S, Chen Z L, Jin A M (2011). Hydrocarbon preservation conditions in marine strata of the Guizhong depression and its margin. Acta Petrol Sin, 32(3): 432–441

Loucks R G, Reed R M, Ruppel S C, Hammes U (2012). Spectrum of pore types and networks in mudrocks and a descriptive classification for matrix-related mudrock pores. AAPG Bull, 96(6): 1071–1098

Lu X C, Li F C, Watson A T (1995). Adsorption measurements in Devonian shales. Fuel, 74(4): 599–603

Nie H K, Bao S J, Gao B, Bian R K, Zhang P X, Wu X L, Ye X, Chen X J (2012). A study of shale gas preservation conditions for the Lower Paleozoic in Sichuan Basin and its periphery. Earth Sci Front, 19(3): 280–294

Nie H K, Bian R K, Zhang P X, Gao B (2014). Micro-types and characteristics of shale reservoir of the Lower Paleozoic in Southeast Sichuan Basin, and their effects on the gas content. Earth Sci Front, 21(4): 331–343

Nie H K, Li D H, Liu G X, Lu Z Y, Hu W, Wang R Y, Zhang G R (2020). An overview of the geology and production of the Fuling shale gas field, Sichuan Basin, China. Ener Geosci, 1(3–4): 147–164

Pan R F, Tang X L, Meng J H, Zhang X M, Gong Y (2014). Shale gas preservation conditions for the Upper Paleozoic in Guizhong Depression. Oil Gas Geol, 35(4): 534–541 (in Chinese)

Roger M S, Neal R O (2011). Pore types in the Barnett and Woodford gas shale: contribution to understanding gas storage and migration pathways in fine-grained rocks. AAPG Bull, 95(12): 2017–2030

Ross D J K, Bustin R M (2009). The importance of shale composition and pore structure upon gas storage potential of shale gas reservoirs. Mar Pet Geol, 26(6): 916–927

Si C S, Zhang R H, Yao G S, Guo Q X, Zhu Z H, Lou Z H, Jin C, Jin A M, Huang L (2016). Tectonism and hydrocarbon preservation condition of Qianbei depression and its margin. J China Univ Min Tech, 45(5): 1010–1022 (in Chinese)

Tan J Q, Weniger P, Krooss B, Merkel A, Horsfield B, Zhang J C, Boreham C J, Graas G V, Tocher B A (2014). Shale gas potential of the major marine shale formations in the Upper Yangtze Platform, South China. Part II: methane sorption capacity. Fuel, 129: 204–218

Tang X L, Jiang S, Jiang Z X, Li Z, He Z L, Long S X, Zhu D Y (2019). Heterogeneity of Paleozoic Wufeng-Longmaxi formation shale and its effects on the shale gas accumulation in the Upper Yangtze Region, China. Fuel, 239: 387–402

Tang X, Jiang Z, Jiang S, Li Z (2016). Heterogeneous nanoporosity of the Silurian Longmaxi Formation shale gas reservoir in the Sichuan Basin using the QEMSCAN, FIB-SEM and nano-CT methods. Mar Pet Geol, 78: 99–109

Wang C, Zhang B Q, Shu Z G, Lu Y C, Lu Y Q, Bao H Y, Li Z, Liu C (2018). Lithofacies types and reservoir characteristics of marine shales of the Wufeng Formation-Longmaxi Formation in Fuling area, the Sichuan Basin. Oil Gas Geol, 39: 485–497 (in Chinese)

Wang R Y, Ding W L, Gong D J, Leng J G (2016). Gas preservation conditions of marine shale in northern Guizhou area: a case study of the Lower Cambrian Niutitang Formation in the Cengong block, Guizhou Province. Oil Gas Geol, 37: 45–55 (in Chinese)

Wang S Q, Chen G S, Dong D Z, Yang G, Lu Z G, Xu Y H, Huang Y B (2009). Accumulation conditions and exploitation prospect of shale gas in the Lower Paleozoic Sichuan Basin. Nat Gas Ind, 29: 51–58 (in Chinese)

Wang Y, Chen J, Hu L, Zhu Y M (2013). Sedimentary environment control on shale gas reservoir: a case study of Lower Cambrian Qiongzhusi Formation in the Middle Lower Yangtze area. J China Coal Soc, 38(5): 845–850 (in Chinese)

Yi J Z, Bao H Y, Zheng A W, Zhang B, Shu Z, Li J, Wang C (2019). Main factors controlling marine shale gas enrichment and high-yield wells in South China: a case study of the Fuling shale gas field. Mar Pet Geol, 103: 114–125

Zeng L B, Lyu W Y, Li J, Zhu L F, Weng J Q, Yue F, Zu K W (2016). Natural fractures and their influence on shale gas enrichment in Sichuan Basin, China. J Nat Gas Sci Eng, 30: 1–9

Zhang J C, Nie H K, Xu B, Jiang S L, Zhang P X (2008). Geological condition of shale gas accumulation in sichuan basin. Nat Gas Ind, 28: 151–156 (in Chinese)

Zhao J H, Jin Z J, Lin C S, Liu G X, Liu K Y, Liu Z B, Zhang Y Y (2019). Sedimentary environment of the Lower Cambrian Qiongzhusi Formation shale in the Upper Yangtze region. Oil & Gas Geol, 40: 701–715 (in Chinese)

Zhao P, Li X Q, Tian X W, Su G P, Zhang M Y, Guo M, Dong Z L, Sun M M, Wang F Y (2014). Study on micropore structure characteristics of Longmaxi Formation shale gas reservoirs in the southern Sichuan Basin. Nat Gas Geosci, 25(6): 947–956 (in Chinese)

Zhao W Z, Li J Z, Yang T, Wang S F, Huang J L (2016). Geological difference and its significance of marine shale gases in South China. Pet Explor Dev, 43(4): 499–510

Zheng H R, Zhang J C, Qi Y C (2020). Geology and geomechanics of hydraulic fracturing in the Marcellus shale gas play and their potential applications to the Fuling shale gas development. Ener Geosci, 1(1–2): 36–46

Zou C N, Du J H, Xu C C, Wang Z C, Zhang B M, Wei G Q, Wang T S, Yao G S, Deng S H, Liu J J, Zhou H, Xu A N, Yang Z, Jiang H, Gu Z D (2014). Formation, distribution, resource potential and discovery of the Sinian-Cambrian giant gas field, Sichuan Basin, SW China. Pet Explor Dev, 41(3): 278–293